

## MINERALOGY AND GEOTHERMOMETRY OF GABBRO-DERIVED LISTVENITES IN THE TISOVITA–IUTI OPHIOLITE, SOUTHWESTERN ROMANIA

GAËLLE PLISSART<sup>§</sup> AND OLIVIER FÉMÉNIAS

*Laboratoire de Géochimie Isotopique et Géodynamique Chimique, DSTE, Université Libre de Bruxelles U.L.B. (CP 160/02),  
 50, avenue Roosevelt, B–1050 Brussels, Belgium, and Laboratoire de Planétologie et Géodynamique, UMR CNRS 6112,  
 UFR de Sciences et Techniques, BP 92208, F–44322 Nantes Cedex 3, France*

MARCEL MĂRUNTIU

*Geological Institute of Romania, 1 Caransebes Street, RO–78344, Bucuresti, Romania*

HERVÉ DIOT

*Université de la Rochelle, av. M. Crépeau, F–17042 La Rochelle Cedex 1, and UMR CNRS 6112,  
 UFR de Sciences et Techniques, BP 92208, F–44322 Nantes Cedex 3, France*

DANIEL DEMAIFFE

*Laboratoire de Géochimie Isotopique et Géodynamique Chimique, DSTE, Université Libre de Bruxelles U.L.B. (CP 160/02),  
 50, avenue Roosevelt, B–1050 Brussels, Belgium*

### ABSTRACT

Gabbros from the Variscan Tisovita–Iuti ophiolite in Romania display the peculiar Cr-rich mica + calcite + quartz mineral association that is typical of listvenites. This metasomatic lithology appears as the end-product of a continuous petrographic series of transformed rocks from amphibolitized gabbros (resulting from an ocean-floor metamorphism) to listvenites. During these different degrees of modification, chromium is immobile and concentrated in the main silicate phases of each stage (amphibole, chlorite and white mica). This process could appear mineralogically and texturally continuous, but chlorite morphology and thermometry suggest two main processes. Listvenite formation characterizes a low-temperature (~300°C) metasomatic stage overprinted on a previously warmer (>450°C) more common process described as ocean-floor metamorphism.

*Keywords:* listvenite, Cr-rich muscovite, chlorite thermometry, ophiolite, metasomatism, ocean-floor metamorphism, Tisovita–Iuti ophiolite, Romania.

### SOMMAIRE

Les gabbros de l'ophiolite varisque de Tisovita–Iuti en Roumanie présentent des faciès particuliers de type listvenite à mica chromifère, calcite et quartz. Ces roches apparaissent comme le produit final d'un continuum pétrographique depuis les gabbros amphibolitisés, classiques du métamorphisme de plancher océanique, jusqu'à leur transformation complète en listvénite. Au cours des différents degrés de cette évolution métasomatique, le chrome est immobile et se concentre dans les différentes phases majeures silicatées, amphibole puis chlorite et mica blanc. Si la métasomatose peut apparaître continue, d'un point de vue minéralogique et textural, le processus semble cependant découplé dans le temps d'après les morphologies et les résultats thermométriques fondés sur les chlorites. La formation de listvénites serait l'aboutissement d'un épisode métasomatique de basse température (~300°C) surimposé au métamorphisme plus classique de plancher océanique, de plus haute température (>450°C).

*Mots-clés:* listvénite, muscovite chromifère, thermométrie sur chlorite, ophiolites, métasomatose, métamorphisme de plancher océanique, ophiolite Tisovita–Iuti, Roumanie.

<sup>§</sup> Aspirant FNRS; E-mail address: gplissar@ulb.ac.be

## INTRODUCTION

Listvenites are uncommon rocks formed by the metasomatic transformation of mafic and ultramafic protoliths to a carbonated lithology (Rose 1837). Their formation refers to the same process that generates beresites, low-temperature metasomatic rocks characterized by the assemblage quartz + white mica + carbonate (ankerite) + pyrite but resulting from the replacement of silicic igneous or sedimentary protoliths (Zharikov *et al.* 2007). In the last decades, the term listvenite (or listwaenite, listwanite, listvanite) has been used in some cases in an inappropriate or restrictive way. However, the “true” listvenite, according to Halls & Zhao (1995), should be considered as a metasomatic rock derived from an ultramafic or a mafic protolith and characterized by the specific assemblage chromian muscovite + quartz + Fe–Mg carbonates + pyrite. The geological interest of such rocks is linked to their likely associated mineralization in precious metals (Au, Co, Sb, Cu, Ni) (*e.g.*, Ash & Arksey 1990a, b, Aydal 1990, Buisson & Leblanc 1985, 1987, Koç & Kadioglu 1996, Nixon 1990, Uçurum 1998, 2000).

Listvenites derived from ultramafic protoliths associated with the Tisovita–Iuti ophiolite, in the southern Carpathians of Romania, can be considered as “true” listvenites according to the definition of Halls & Zhao (1995). Nevertheless, in contrast with classical examples that imply the presence of serpentine in the protolith, some listvenites from Romania are also directly derived from gabbroic protoliths. To constrain the geotectonic environment of formation of these uncommon mafic-rock-derived listvenites, rock-forming minerals and geothermobarometric conditions of formation have been studied. The composition of chromian chlorite and chromian mica has been determined by electron-microprobe analysis and is utilized to infer P–T conditions from (1) empirical geothermobarometers and (2) mineral equilibria using Berman’s thermodynamic software winTWQ 2.3 (Berman 1991) with the thermodynamic data of Vidal *et al.* (2001) on chlorite end-members and of Vidal & Parra (2000) on chlorite–phengite end-members. With this approach, we document the environment of formation of this example of gabbro-derived listvenites.

## BACKGROUND INFORMATION

Listvenites are commonly associated with ophiolites (Buisson & Leblanc 1987, Ash & Arksey 1990a, Auclair *et al.* 1993, Halls & Zhao 1995, Koç & Kadioglu 1996, Uçurum 2000, Akbulut *et al.* 2006, Tsikouras *et al.* 2006) and occasionally with greenstone belts (Kishida & Kerrich 1987, Béziat *et al.* 1998). Their formation is classically attributed to carbonatization in presence of K-bearing fluids (Halls & Zhao 1995). The formation of listvenite can be described as a three-stage metasomatic

process in a serpentine-rich protolith: 1) carbonatization (Halls & Zhao 1995), *e.g.*,  $\text{Srp} + 3 \text{CO}_2 = 3 \text{carbonate} + 2 \text{Qtz} + 2 \text{H}_2\text{O}$ , 2) silicification, external contribution of silica or silica released in reaction (1), and 3) mica formation, *e.g.*,  $3 \text{Ab} + \text{K}^+ + 2 \text{H}^+ = \text{Ms} + 6 \text{Qtz} + \text{Na}^+$  (Kishida & Kerrich 1987).

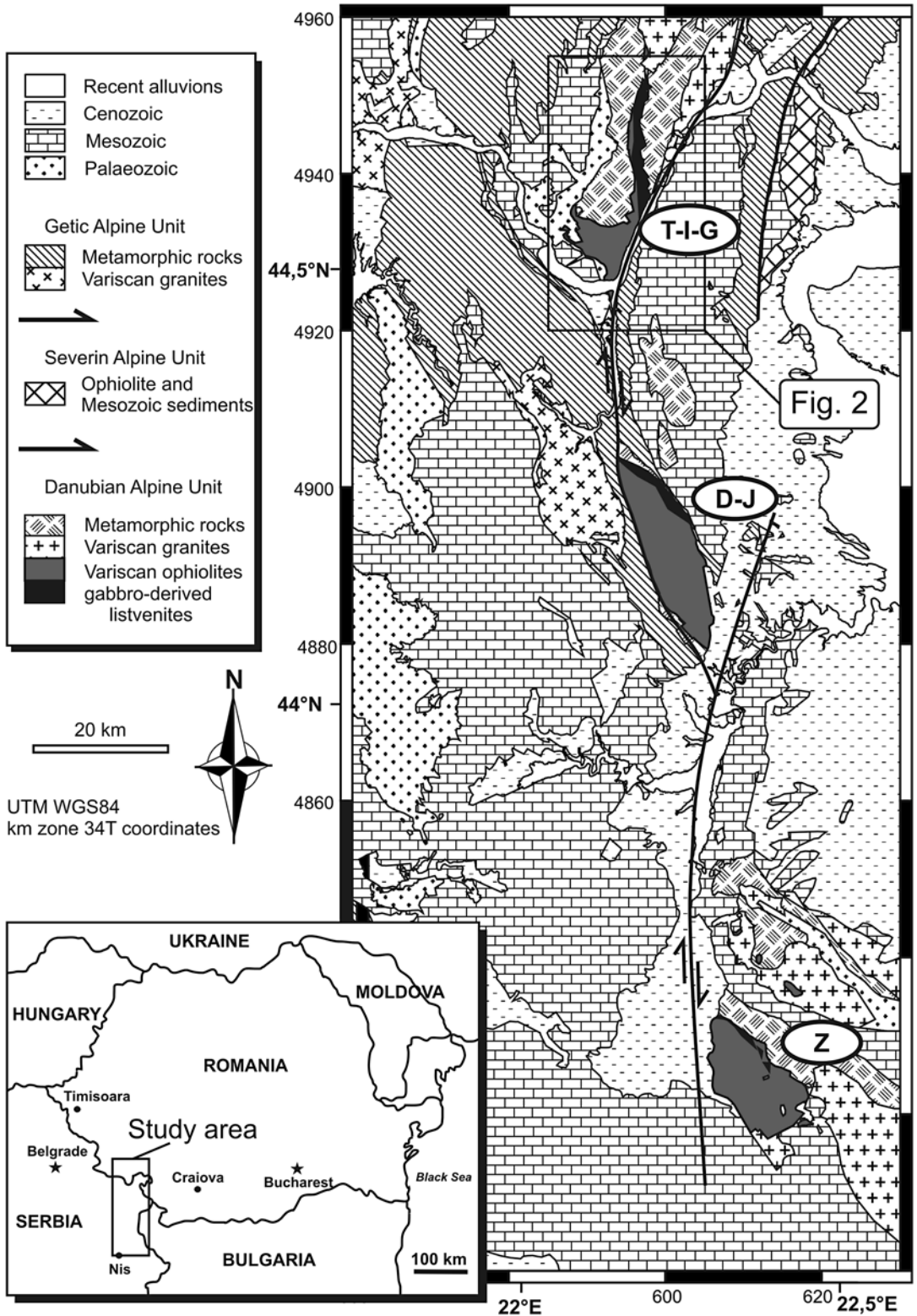
The latter stage requires an external source of K that could be linked to deuteritic fluids associated with felsic intrusions (Ash 2001) or to seawater-derived fluids. Consequently, ophiolite-related formation of listvenite can occur in two distinct geotectonic environments; subsequent to the obduction of the ophiolite (*e.g.*, in dismembered ophiolites in British Columbia: Ash 2001), where it is considered as a continental mechanism, and in an oceanic domain in a pre- or syn-obduction context (Kishida & Kerrich 1987, Buisson & Leblanc 1987, Auclair *et al.* 1993, Tsikouras *et al.* 2006), which could be considered an unusual expression of ocean-floor metamorphism.

## GEOLOGICAL SETTING

The Tisovita–Iuti ophiolite is located in the Almaj Mountains in southern Carpathians of Romania (22.2°E, 44.5°N); it may be associated with the ophiolitic complexes of Deli Jovan and Zaglavak in Serbia (Fig. 1). The accretion of the “Danubian oceanic crust” has been dated to the Early Devonian (U–Pb zircon age of  $405 \pm 2.6$  Ma; Zakariadze *et al.* 2006). The three massifs constitute a “Danubian Ophiolite”, which corresponds to the relics of a Variscan oceanic domain outcropping along a 160-km-long single tectonic suture dismembered by the Oligocene Cerna–Timok dextral strike-slip fault.

The South Carpathian Alpine belt consists of the Upper Cretaceous stacking of two major units (Getic and Danubian, composed of a crystalline basement locally covered by Paleozoic and Mesozoic sediments) thrust upon the Moesian cratonic platform during the Tertiary period. These units were partly covered by Cenozoic sediments, marked by a major unconformity. The various Eoalpine (Cretaceous) Danubian nappes have been subdivided into Upper and Lower Danubian (Berza *et al.* 1983, 1994) based on their Mesozoic cover (Stănoiu 1973, Kräutner *et al.* 1981). The Upper Danubian nappe, outcropping in the Almaj Mountains, is composed of two principal Variscan terranes: Poiana Mraconia and Neamțu (Fig. 2). The Neamțu unit is essentially composed of metapelites, paragneisses

FIG. 1. Schematic geological map of the dismembered “Danubian ophiolite” (T–I–G: Tisovita–Iuti–Glavica, Romania, D–J: Deli Jovan, and Z: Zaglavak, Serbia) in the southern Carpathians.



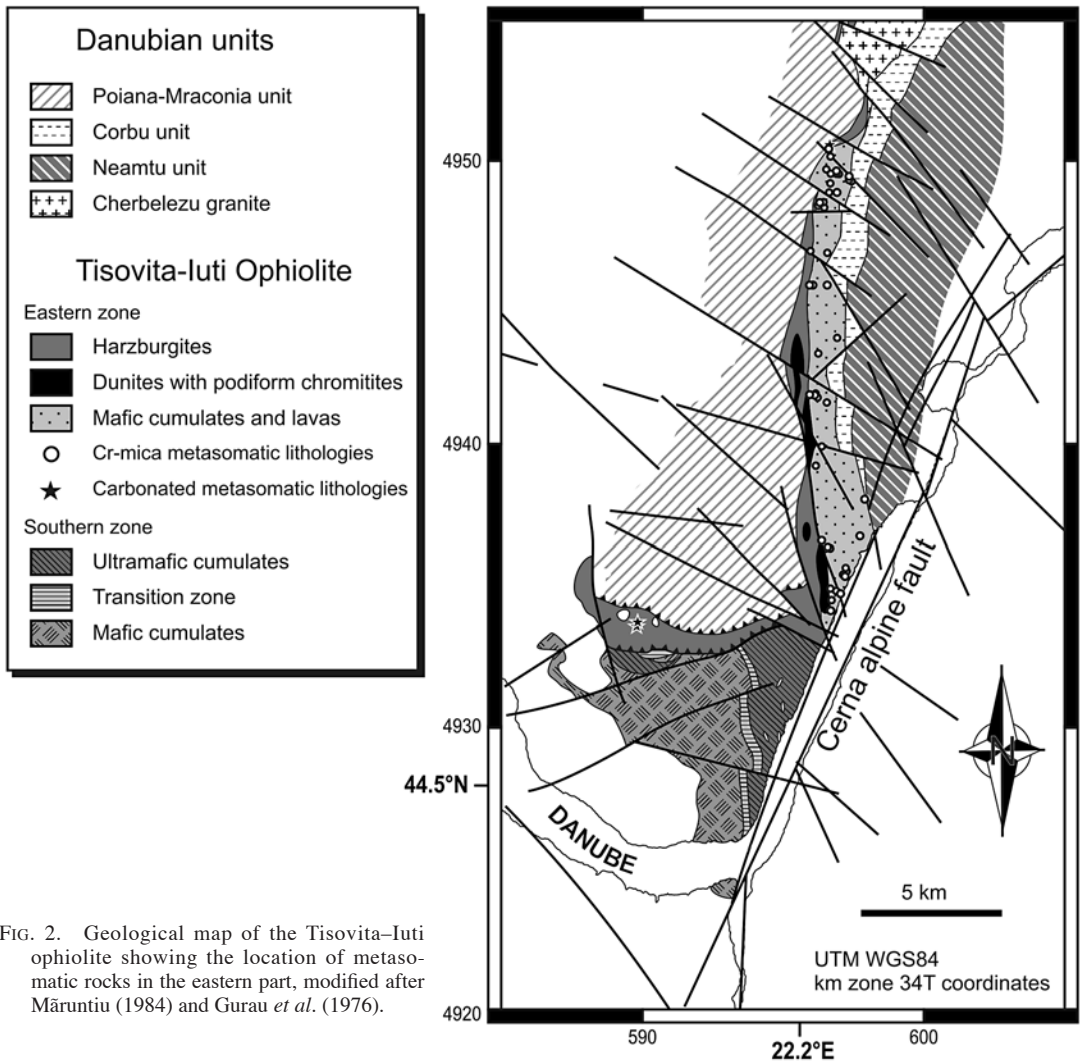


FIG. 2. Geological map of the Tisovita–Iuti ophiolite showing the location of metasomatic rocks in the eastern part, modified after Mărunțiu (1984) and Gurau *et al.* (1976).

and granitic bodies, forming an important migmatitic complex. This unit is characteristically affected by a medium-pressure – high-temperature amphibolite-grade metamorphism. The Poiana–Mraconia unit is composed of paragneisses and amphibolites. The area is intruded by (1) large, elongate, late-orogenic plutons (*i.e.*, the Cherbezezu and Sfârdin plutons) that belong to the Carboniferous episode of synorogenic magmatism (Plissart *et al.* 2007), (2) a post-orogenic high-K calc-alkaline Almaj dykes swarm (Féménias 2003, Féménias *et al.* 2008) and (3) some small Mesozoic anorogenic alkaline syenites. The tectonic contact between these two major metamorphic units corresponds to the structural position of the Tisovita–Iuti ophiolitic complex (Fig. 2).

Variations in lithology allow us to distinguish two parts in the Tisovita–Iuti ophiolitic massif (Mărunțiu 1984) (Fig. 2). (1) The southern part, a low-dip stack, consists of ultramafic cumulates (layered dunites and serpentinites) and a layered sequence of mafic cumulates (gabbros, olivine gabbros and troctolites) cross-cut by undeformed gabbros (Mărunțiu *et al.* 1997). The upper mantle section and the effusive unit of typical ophiolites are missing. (2) The eastern part is composed of a complete ophiolitic section, from west to east, and outcrops in a narrow reverse high-dip slice. Upper mantle lithologies consist of serpentinitized harzburgites and lenses of dunite and podiform chromitite. The Moho transition from harzburgites to gabbros is well defined and observable in outcrops in the Mraconia River. The

crustal unit is dominated by metagabbros with various textures (undeformed, flaser, fine-grained and pegmatitic). Plagiogranites occur as dykes and bodies up to a hundred meters in width. Their field relations with gabbros and their low contents of incompatible elements (work in progress) favor a genesis by partial melting of pre-existing gabbros. Basaltic dykes, cross-cutting the gabbros, evolve to a true effusive unit at the top of the ophiolite section, well represented in Serbia (Deli Jovan and Zaglavak massifs, Fig. 1). Although local quench-fragmented hyaloclastite breccia occurs in Serbia, a classical sheeted dyke complex and pillow structures have not been observed owing to the strong deformation at the top of the ophiolitic sequence.

#### FIELD OCCURRENCES AND PETROGRAPHIC DESCRIPTIONS

The Eastern part of the Tisovita-Iuti ophiolite is characterized by an early hydrothermal ocean-floor metamorphism and a later, localized (Fig. 2) but well-developed metasomatic overprint event that affected the ultramafic, mafic and silicic rocks. The metasomatism of ultramafic rocks produced a strongly transformed, greyish, yellowish and chromian-white-mica-bearing carbonated lithology that corresponds to a listvenite *s.s.* (Halls & Zhao 1995), whereas metasomatism generated white epidote-rich beresitic rocks at the expense of plagiogranites. Mafic lithologies (gabbro-derived) were transformed into a white to greenish smooth, glittering rock (Gurau *et al.* 1976) that is related to listvenite *s.s.* The green color is attributed to chromian white mica and is easily recognizable. Listvenite formation affected both deformed and undeformed areas a hundred meters wide inside the Romanian gabbroic part of the crustal section. Comparable gabbro-derived listvenites were also found in the Eastern part of the Serbian massifs of

Deli Jovan and Zaglavak (Fig. 1). A detailed field and petrographic study of the Tisovita-Iuti gabbro-derived metasomatic lithologies emphasizes the existence of a sequence from amphibolitized gabbro ("protolith") to true chromian-white-mica-bearing listvenite. Five main assemblages were defined (Table 1).

The first assemblage (Table 1, Fig. 3a: Amp-G s1 = epidote-bearing amphibolitized gabbro) contains green magnesiohornblende (generally twinned) in equilibrium with an intermediate plagioclase and epidote. Plagioclase is classically replaced by a secondary assemblage of mica + albite + epidote. This alteration affects the core of the crystals following a pre-existing zonation. White mica and chlorite are rare and not chromiferous.

This facies evolves progressively to the second assemblage (Table 1, Fig. 3b: Amp-G s2 = clinozoisite-bearing amphibolitized gabbros), which contains increased amounts of actinolite, chlorite, clinozoisite and zoisite. Actinolite is more abundant than green hornblende and appears as pale green large crystals or as a rim on a hornblende. Colorless euhedral clinozoisite replaces plagioclase. Chlorite is mainly colorless and appears as well-developed tabular crystals more than 1 mm in size, or as flakes that replace green amphibole. White mica is locally present as well-developed tabular crystals. Carbonates have occasionally been observed in replacement of actinolite.

The third assemblage (Table 1, Fig. 3c: Czo-G s3 = (clinozoisite + chlorite)-bearing amphibolitized gabbros) is characterized by the complete disappearance of magnesiohornblende and epidote and an increase in the content of chlorite and white mica that become chromiferous. Clinozoisite generally forms small aggregates of anhedral grains in the sodic plagioclase. Chlorite and mica display the same habit as in clinozoisite-bearing amphibolitized gabbros (Amp-G s2),

TABLE 1. ASSEMBLAGES IN THE MAIN METASOMATIC LITHOLOGIES OF THE T-I OPHIOLITE DEFINED FROM MODAL PROPORTIONS OF THE MINERAL PHASES

		amphibole		ab	chl	epidote group			white mica		cal	qtz	tn	rt	sulf	
		mhb	act			ep	czo	zo	no Cr	+ Cr						
Amp-G s1	epidote-bearing amphibolitized gabbro	++++	+	+++++	+	++	-	-	+	-	-	-	-	-	-	-
Amp-G s2	clinozoisite-bearing amphibolitized gabbro	+++	++	++++	++	+	++	+	++	-	+	+	+	-	+	
Czo-G s3	(clinozoisite + chlorite)-bearing amphibolitized gabbro	+	+++	+++	+++	-	+++	++	++	+	+	-	+	-	+	
Zo-G s4	(zoisite + chlorite)-bearing amphibolitized gabbro	-	+	+	++++	-	-	++++	-	+++	++	+	+	-	+	
List s5	listvenite	-	-	+	++++	-	-	+++++	-	+++	+++	+	+	+	+	+
Pl-y	plagiogranite	-	-	++++	+	++	+	-	+	-	+	+++	-	-	-	-

but appear also in close microcrystalline associations. Calcite veinlets cross-cut the rocks, which suggests a late formation.

The strong increase of zoisite, chlorite and chromian white mica and the progressive disappearance of actinolite and clinozoisite characterize the fourth assemblage (Table 1: Zo-G s4 = (zoisite + chlorite)-bearing amphibolitized gabbros). These deeply transformed rocks resemble the fifth assemblage (Table 1, Fig. 3d: List s5 = listvenites *s.s.*) except that calcite, rutile and sulfides (that characterize the final listvenitic stage) are more scarce or absent. Listvenites *s.s.* are principally composed of zoisite in greyish microcrystalline aggregates, disseminated calcite, white mica + chlorite in a fine-grained association and quartz. This assemblage completely overprints the original magmatic texture. Local enrichment in chromium is characterized by the occurrence of blue-green pleochroic chromian white mica, colorless chromian chlorite and chromian zoisite. An unusual Cr-diffusion aureole (Fig. 3e) is observed around a relict chromium-rich phase (*e.g.*, spinel).

Numerous plagiogranitic intrusions composed of quartz + albite (Table 1: Pl- $\gamma$ ) are present as stocks or dykes in the mafic series of the Tisovita–Iuti ophiolite. They commonly display postmagmatic metasomatic modifications, comparable to those leading to listvenite formation, characterized by the common breakdown of plagioclase and new development of white mica and calcite, defining the so-called beresites (Zharikov *et al.* 2007). The formation of beresites affecting the felsic rocks is similar to the transformation of gabbros and ultramafic lithologies to listvenites. The two processes will be discussed together.

#### MINERAL COMPOSITION

The major-element composition of the main mineral phases was determined with the electron microprobes (Cameca SX50 and SX100) at the CAMPARIS center (Université Paris VII) using WDS and a combination of natural and synthetic mineral standards. Operating conditions were: beam current 10 nA and 15 nA for each instrument, respectively, an accelerating voltage of 15 kV for both instruments, with a counting time of 10 s per element.

#### *Amphibole*

The  $\text{Fe}^{2+}:\text{Fe}^{3+}$  ratio of all the amphiboles was calculated following Schumacher's method (Appendix in Leake *et al.* 1997); thus we estimated limits of maximum and minimum values of ferric ion content on the basis of permissible and usual site-occupancies in an amphibole. All amphiboles from the mafic lithologies of the Tisovita–Iuti ophiolite are calcic according to the IMA classification (Leake *et al.* 1997). They range from magnesiohornblende to actinolite (Table 2, Fig. 4a). The  $\text{Mg}\#$  [ $100\text{Mg}/(\text{Mg} + \text{Fe}^{2+})$ ] varies between 74 and

89.2 (average value: 84). The Ti content is commonly lower than 0.2 *apfu*. The Cr content varies between 0 and 0.15 *apfu* (Table 2, Fig. 4b). The highest values (1.1 to 1.3 wt%  $\text{Cr}_2\text{O}_3$ ) were found in zoisite-bearing gabbros (Table 2, Fig. 4b), whereas the amphibole of amphibolitized gabbros s1 and s2 displays low contents, with only a local enrichment (up to 0.8 wt%  $\text{Cr}_2\text{O}_3$ ). The composition of the amphibole evolves along the primary evolutionary sequence (Fig. 4a). The  $\text{Mg}\#$  increases from the first stage of pyroxene replacement by a green hornblende (64 to 73 for Amp-G s1) to the other stages of the sequence (74 to 89 for Amp-G s2, 82 to 88 for Czo-G s3 and Zo-G s4). The Si content also changes along the sequence, displaying a strong increase from amphibolitized gabbros (6.7 to 7.9 *apfu* for Amp-G s1 and s2) to the more altered stages (7.6 to 7.9 for Czo-G s3 and Zo-G s4), reflecting the composition of the neofomed actinolite.

The range of amphibole composition in the Tisovita–Iuti ophiolitic gabbros is quite comparable (Fig. 4a) to those of classical ophiolites like Trinity (Lécuyer *et al.* 1990) and Lizard (Hopkinson & Roberts 1995). Comparable compositions have also been observed in present-day ocean-floor materials (Fig. 4a) from the southwestern Indian Ridge (Hole 735B, gabbros from Atlantis II Transform, Stakes *et al.* 1991, Vanko & Stakes 1991, Robinson *et al.* 2002) and Mid-Atlantic Ridge (Holes 921 to 924, hydrothermal veins in gabbros from the Kane Transform, Dilek *et al.* 1997).

#### *Epidote-group minerals*

Epidote-group minerals of the Tisovita–Iuti suite can be subdivided into three distinct groups on the basis of the  $X_{\text{Fe}^{3+}}$  [ $\text{Fe}^{3+}/(\text{Fe}^{3+} + \text{Al}^{3+} - 2 + \text{Cr}^{3+})$ ] content of the M3 site of the structural formula (Table 3, Fig. 5a): (1) epidote *s.s.* ( $X_{\text{Fe}^{3+}} > 0.5$ ) is present in epidote-bearing amphibolitized gabbros (Amp-Gs 1) and plagiogranites (Pl- $\gamma$ ); (2) clinozoisite ( $0.15 < X_{\text{Fe}^{3+}} < 0.5$ ) occurs in clinozoisite and clinozoisite + chlorite amphibolitized gabbros (Amp-G s2 and Czo-G s3); (3) zoisite ( $X_{\text{Fe}^{3+}} < 0.15$ ) is restricted to zoisite + chlorite amphibolitized gabbros (Zo-G s4) and listvenites (List s5). The Cr content of zoisite reaches 1.24 wt %  $\text{Cr}_2\text{O}_3$  in listvenites and chromian-mica-bearing gabbros. Epidote displays a wide range of  $\text{Fe}^{3+}$ -for- $\text{Al}^{3+}$  substitution (Fig. 5b), which is not commonly observed in comparable geological environments. A few compositions (Fig. 5b) plot outside the typical range of substitution and display lower sum of  $\text{Al}^{3+} + \text{Fe}^{3+}$ , in agreement with their abnormally high Si content.

In comparison with the Tisovita–Iuti ophiolite, gabbros from ODP Hole 735B (Cannat *et al.* 1991) and East Taiwan ophiolite (Liou & Ernst 1979) do not contain zoisite. Iron-rich epidote (epidote *s.s.* in Fig. 5) has not been observed in the Limousin ophiolite (Berger *et al.* 2005, J. Berger, pers. commun., 2008). On the contrary, the Trinity ophiolite is characterized by

the absence of true clinozoisite (Lécuyer *et al.* 1990). The Fe content in epidote from Tisovita–Iuti decreases along the “petrological” sequence: epidote *s.s.* occurs in slightly altered gabbros, whereas zoisite characterizes the more transformed rocks.

### Chlorite

The calculation of a structural formula for a chlorite is complex because the proportion of vacancies in the octahedral site varies with the  $\text{Fe}^{2+}:\text{Fe}^{3+}$  ratio, according to the tri-dioctahedral substitution as defined by Foster (1962). As the  $\text{Fe}^{2+}:\text{Fe}^{3+}$  ratio cannot be determined with an electron microprobe, and the existence of octahedral vacancies in the crystallographic network cannot really be assessed, a simple calculation to obtain the structural formula is impossible. However, the  $\text{Fe}^{3+}$  content of the chlorite is typically less than 15% of  $\text{Fe}_{\text{tot}}$  and is not related to the oxygen fugacity conditions but rather to crystal-chemical constraints (Dyar *et al.* 1992, Zane *et al.* 1998). Consequently, the structural formula of the analyzed chlorites has been calculated considering  $\text{Fe}^{2+} = \text{Fe}_{\text{tot}}$ . The possibility of octahedral vacancies in

chlorites is hotly debated: some authors (*i.e.*, Shau *et al.* 1990, Jiang *et al.* 1994) have claimed that calculated vacancies are only an artefact linked to the presence of interstratified mineral associations or fine-grained intergrown minerals. We have checked for these possible interstratifications in the Tisovita–Iuti chlorites by using (i) the criteria of Foster (1962), defined as  $\text{Na}_2\text{O} + \text{K}_2\text{O} + \text{CaO} < 0.5 \text{ wt\%}$  (see Hillier & Velde 1991, and Jiang *et al.* 1994), (ii) a variety of bi-element correlation diagrams proposed by Shau *et al.* (1990) and Jiang *et al.* (1994), and (iii) several criteria to exclude contaminated compositions, as defined by Vidal & Parra (2000) and Vidal *et al.* (2001). All these criteria are fulfilled for the Tisovita–Iuti chlorites (Table 4), which allows us to calculate the structural formulae with octahedral vacancies. Site occupancy is calculated according to Vidal & Parra (2000), with  $\text{Cr}^{3+}$  incorporated at the *M4* interlayered  $^{\text{VI}}\text{Al}$  site as described by Bish (1977), Phillips *et al.* (1980) and Rule & Bailey (1987, in Bailey 1988). The labels applied to chlorite-group minerals in this work correspond to the thermodynamic end-members of Vidal & Parra (2000) and Vidal *et al.* (2001, 2005) (Table 5). The names of those end members that do not

TABLE 2. REPRESENTATIVE COMPOSITIONS AND STRUCTURAL FORMULAE OF T–I AMPHIBOLES

Name	Amp-G s1					Amp-G S2					Czo-G S3			Zo-G S4	
	core Mhb	rim Act	core Mhb	rim Mhb	Mhb	Act	core Mhb	rim Act	Mhb	Act	Act	Act	Act	Act	Act
$\text{SiO}_2$ wt%	51.76	55.75	49.29	49.77	48.29	54.00	48.78	56.98	52.02	54.06	55.87	57.23	56.17	54.41	53.73
$\text{TiO}_2$	0.30	0.00	0.53	0.45	0.40	0.10	0.80	0.02	0.07	0.12	0.58	0.04	0.04	0.11	0.13
$\text{Al}_2\text{O}_3$	4.62	0.63	8.49	8.81	9.15	3.38	10.13	0.63	7.11	3.94	2.25	2.22	3.30	2.88	3.40
$\text{Cr}_2\text{O}_3$	0.12	0.00	0.03	0.02	0.05	0.00	0.06	0.07	0.52	0.79	0.23	0.12	0.02	1.12	1.32
FeO	10.53	8.36	11.91	12.09	10.87	8.61	9.37	6.59	6.04	4.44	4.68	4.69	5.75	5.87	6.54
MnO	0.15	0.23	0.15	0.23	0.19	0.15	0.15	0.14	0.15	0.16	0.06	0.14	0.08	0.19	0.10
MgO	16.46	19.36	13.78	13.75	14.78	17.55	14.99	20.09	18.10	20.62	20.22	19.60	19.29	18.39	17.41
CaO	12.00	13.00	11.58	11.86	11.30	12.63	11.44	12.97	12.06	11.95	13.46	13.18	13.38	13.16	12.94
$\text{Na}_2\text{O}$	0.80	0.12	1.20	1.38	1.69	0.56	1.64	0.11	1.19	0.71	0.38	0.30	0.59	0.35	0.43
$\text{K}_2\text{O}$	0.12	0.00	0.42	0.27	0.21	0.03	0.21	0.01	0.09	0.04	0.05	0.00	0.05	0.00	0.04
Sum	96.87	97.45	97.53	98.91	96.94	97.03	97.57	97.59	97.35	96.83	97.89	97.51	98.85	96.49	96.21
Si <i>apfu</i>	7.430	7.875	7.114	7.101	6.962	7.674	6.943	7.954	7.291	7.531	7.751	7.918	7.744	7.709	7.674
$^{\text{IV}}\text{Al}$	0.570	0.104	0.886	0.899	1.038	0.326	1.057	0.046	0.709	0.469	0.249	0.082	0.256	0.291	0.326
$^{\text{VI}}\text{Al}$	0.211	0.000	0.558	0.583	0.518	0.240	0.642	0.057	0.466	0.178	0.118	0.280	0.280	0.190	0.246
Ti	0.033	0.000	0.057	0.048	0.044	0.011	0.085	0.002	0.007	0.013	0.060	0.004	0.004	0.011	0.014
Cr	0.013	0.000	0.003	0.002	0.005	0.000	0.006	0.008	0.058	0.087	0.025	0.013	0.002	0.126	0.149
$\text{Fe}^{3+}$ calc.	0.109	0.017	0.069	0.051	0.135	0.019	0.083	0.002	0.067	0.110	–	–	–	–	–
$\text{Fe}^{2+}$ calc.	1.264	0.988	1.438	1.443	1.311	1.023	1.115	0.769	0.708	0.518	0.543	0.543	0.663	0.696	0.781
Mn	0.019	0.028	0.018	0.028	0.023	0.018	0.018	0.016	0.017	0.019	0.007	0.016	0.010	0.023	0.012
Mg	3.523	4.076	2.965	2.925	3.176	3.718	3.180	4.180	3.782	4.282	4.182	4.042	3.964	3.885	3.706
Ca	1.829	1.891	1.790	1.813	1.746	1.923	1.744	1.939	1.811	1.784	2.000	1.953	1.976	1.997	1.980
Na	0.224	0.033	0.336	0.381	0.472	0.155	0.452	0.029	0.322	0.193	0.101	0.080	0.159	0.097	0.119
K	0.021	0.000	0.077	0.049	0.038	0.005	0.038	0.002	0.016	0.007	0.009	0.000	0.009	0.000	0.006
Mg#	0.74	0.81	0.67	0.67	0.71	0.78	0.74	0.85	0.84	0.89	0.89	0.88	0.86	0.85	0.83

The formula, expressed in atoms per formula unit, is calculated on the basis of 28 atoms of oxygen.  $\text{Mg\#} = \text{Mg}/(\text{Mg} + \text{Fe}^{2+})$ ; the amount of  $\text{Fe}^{2+}$  and  $\text{Fe}^{3+}$  was calculated according to the appendix of Schumaker in Leake *et al.* (1997). The analyses were done with an electron microprobe. Symbols: Mhb: magnesiohornblende, Act: actinolite.

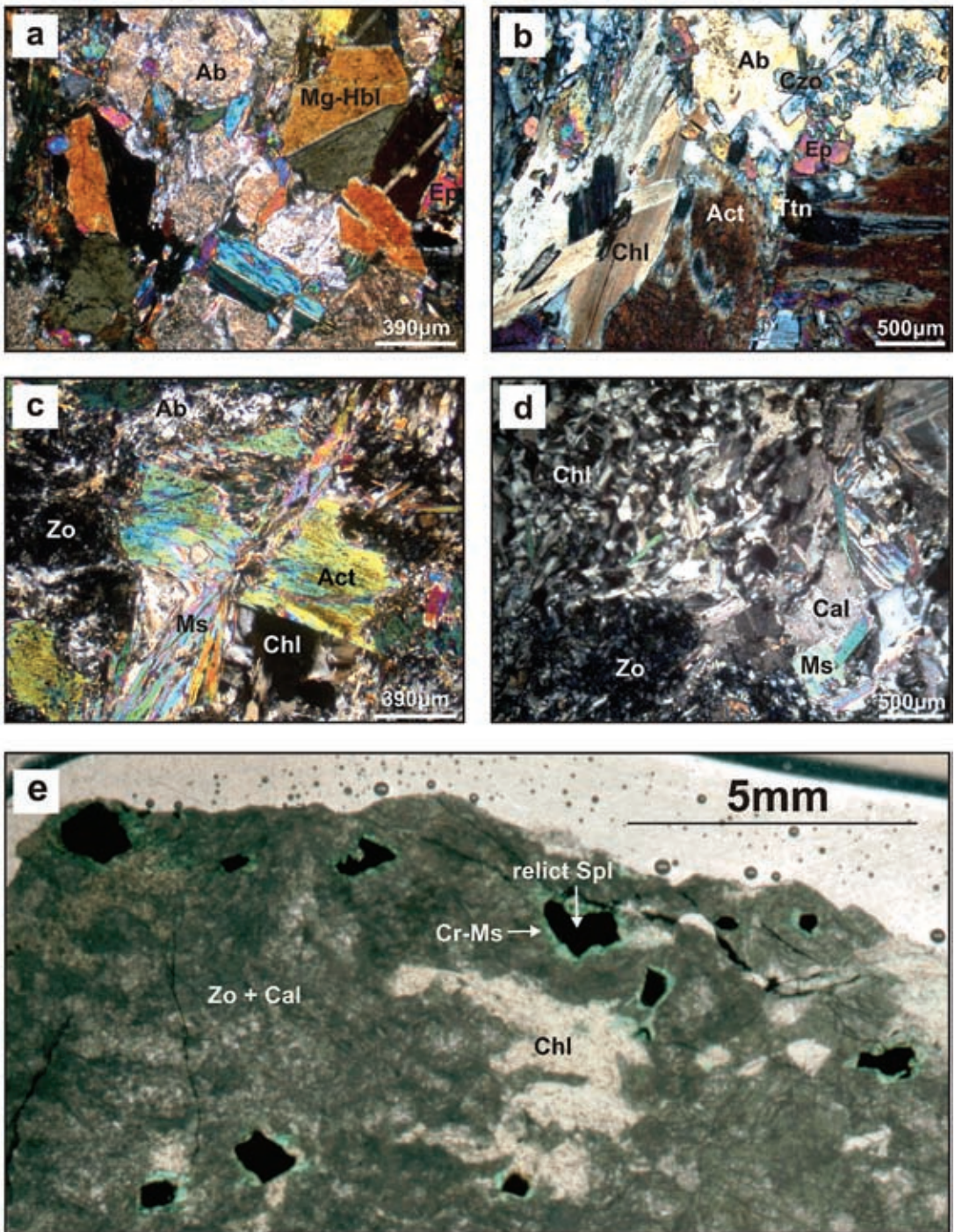


FIG. 3. Photomicrographs (a–d: crossed-polarized transmitted light, e: thin section scanned) of various assemblages (a) Amp–G s1, and (b) Amp–G s2. Note the large tabular grains of chlorite corresponding to the high-T hydrothermal metamorphism event (c) Czo–G s3 and (d) List s5. Note the small grains of chlorite corresponding to the low-T metasomatic event. (e) List s5: note the Cr diffusion aureole around relict spinel. Symbols: Ab: albite, Act: actinolite, Cal: calcite, Chl: chlorite, Czo: clinozoisite, Ep: epidote *s.s.*, Mg–Hbl: magnesian hornblende, Ms: muscovite, Ttn: titanite, Zo: zoisite.

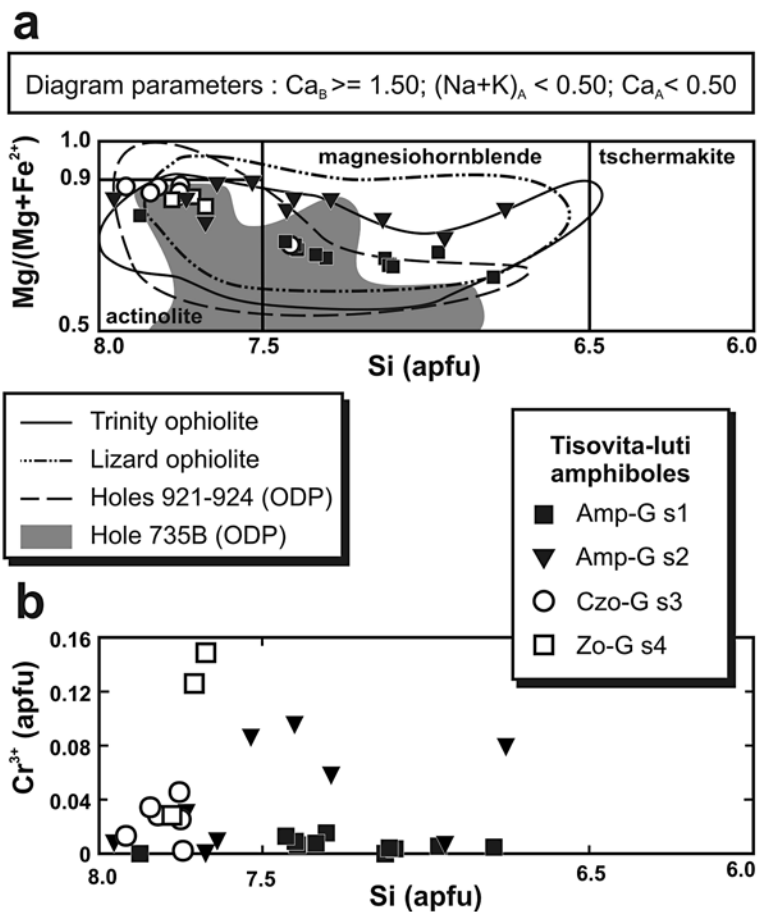


FIG. 4. (a) Composition of Tisovita–Iuti amphiboles from various assemblages and comparison with ancient and modern oceanic occurrences (nomenclature after Leake *et al.* 1997). Compilation from 1: Hole 735B ODP, Atlantis II Transform (gabbros), Southwest Indian Ridge (Stakes *et al.* 1991, Vanko & Stakes 1991, Robinson *et al.* 2002), 2: Holes 921 to 924 ODP (hydrothermal veins in gabbros), Kane Transform, Mid-Atlantic Ridge (Dilek *et al.* 1997), 3: Cap Lizard ophiolite (gabbros), U–K (Hopkinson & Roberts 1995), 4: Trinity ophiolite, California (gabbros and sheeted dyke complex) (Lécuyer *et al.* 1990). (b) Cr contents found in the Tisovita–Iuti amphiboles.

correspond to IMA-sanctioned terminology are shown in quotation marks.

In the Tisovita–Iuti suite, the chlorite is trioctahedral; its composition can be expressed as a linear combination of clinochlore, amesite and sudoite end-members for gabbro-derived lithologies, and essentially of clinochlore and “daphnite” end-members for plagiogranites (Table 4, Fig. 6a). All analyzed grains of chlorites are strongly magnesian (Fig. 6b), which minimizes the errors generated by assuming  $Fe^{2+} = Fe_{tot}$ . The  $Mg/(Mg + Fe_{tot})$  value varies between 0.76 and 0.88 for chlorite of listvenites and metasomatic gabbros, and between 0.54 and 0.66 for chlorite of plagiogranites

(Fig. 6a). The high  $Cr^{3+}$  content (up to 8.45 wt%  $Cr_2O_3$ ) of the chlorites from the (zoisite + chlorite)-bearing amphibolitized gabbros (Zo–G s4) and the listvenites (List s5) is comparable to that of chromian chlorite at other localities (Phillips *et al.* 1980) (Fig. 6c).

The Tisovita–Iuti chlorites display higher Mg contents than those from modern oceanic occurrences [gabbros from Hole 735B ODP (Stakes *et al.* 1991, Vanko & Stakes 1991, Robinson *et al.* 2002); hydrothermal veins in gabbros from Holes 921 to 924 ODP (Dilek *et al.* 1997); upper crust from Hole 504B ODP (Alt *et al.* 1996); Kane Transform + Trans-Atlantic Geotraverse (TAG), + Galapagos + East Pacific Ridge

TABLE 3. REPRESENTATIVE COMPOSITIONS AND STRUCTURAL FORMULAE OF T-I EPIDOTE-GROUP MINERALS

Name	Amp-G s1		Amp-G s2				Czo-G s3			Zo-G s4		List s5		Pl-y	
	Ep	Ep	Czo	Czo	Czo	Zo	Czo	Czo	Czo	Zo	Zo	Zo	Zo	Ep	Ep
SiO <sub>2</sub> wt%	40.47	37.55	38.91	38.05	38.80	39.25	38.40	38.02	38.92	39.92	39.62	43.20	40.23	38.31	39.27
TiO <sub>2</sub>	0.06	0.16	0.00	0.10	0.10	-	0.11	0.10	0.09	0.07	0.03	-	0.03	0.09	0.01
Al <sub>2</sub> O <sub>3</sub>	25.41	25.31	29.86	28.21	27.76	31.65	28.28	28.16	28.30	33.79	32.76	31.44	33.26	26.35	31.21
Cr <sub>2</sub> O <sub>3</sub>	0.11	0.05	-	-	0.03	0.01	0.59	1.24	0.18	-	0.46	0.01	0.01	0.02	-
FeO	8.73	9.70	4.86	6.58	6.53	1.95	6.07	5.19	6.08	0.38	1.29	0.43	0.88	9.02	2.77
MnO	0.17	0.12	0.16	0.18	0.11	0.00	0.16	0.04	0.08	0.06	0.02	0.00	0.03	0.23	0.03
MgO	0.07	0.01	0.07	0.06	0.07	0.02	0.01	0.03	0.04	0.02	0.00	0.06	0.20	0.03	0.00
CaO	21.90	23.83	23.93	24.47	23.20	24.32	24.00	24.15	24.57	25.35	24.97	23.78	24.64	22.96	24.19
Na <sub>2</sub> O	0.03	-	-	-	-	-	-	-	0.02	0.06	-	0.01	0.02	0.03	0.02
K <sub>2</sub> O	0.05	-	0.01	-	0.01	-	0.05	-	-	-	0.02	0.02	0.03	-	-
F	-	0.09	-	-	-	-	0.05	-	0.11	-	0.03	0.06	0.02	-	-
Cl	-	0.05	-	0.01	-	-	-	0.02	0.01	0.01	-	-	-	-	-
Sum	97.00	96.88	97.79	97.64	96.62	97.20	97.71	96.93	98.38	99.66	99.20	99.01	99.35	97.05	97.51
Si <i>apfu</i>	3.144	2.966	2.984	2.951	3.028	3.010	2.970	2.967	2.997	2.980	2.975	3.212	3.008	2.989	3.008
Ti	0.003	0.009	-	0.006	0.006	-	0.006	0.006	0.005	0.004	0.002	-	0.002	0.005	-
<sup>VI</sup> Al	2.327	2.356	2.699	2.578	2.554	2.860	2.578	2.589	2.568	2.973	2.899	2.756	2.931	2.423	2.818
Cr	0.007	0.003	0.000	0.000	0.002	0.001	0.036	0.076	0.011	0.000	0.027	0.000	0.001	0.001	0.000
Fe <sup>3+</sup> calc.	0.567	0.641	0.312	0.427	0.426	0.125	0.392	0.338	0.392	0.024	0.081	0.027	0.055	0.589	0.178
Mn <sup>3+</sup> calc.	0.011	-	-	-	0.007	-	-	-	0.005	-	-	-	0.002	-	0.002
Fe <sup>2+</sup> calc.	-	0.022	0.027	0.026	-	-	0.032	0.023	-	-	0.022	-	-	0.047	-
Mn <sup>2+</sup> calc.	-	0.008	0.010	0.012	-	-	0.011	0.003	-	0.004	0.001	-	-	0.015	-
Mg	0.008	0.002	0.008	0.006	0.008	0.002	0.002	0.003	0.004	0.002	-	0.006	0.022	0.004	-
Ca	1.823	2.019	1.969	2.036	1.940	1.998	1.991	2.021	2.027	2.028	2.011	1.894	1.974	1.922	1.985
F	-	0.005	-	-	-	-	0.002	-	0.006	-	0.002	0.003	0.001	-	-
Cl	-	0.001	-	-	-	-	-	-	-	-	-	-	-	-	-
X Ep	0.63	0.641	0.308	0.425	0.434	0.127	0.39	0.337	0.404	0.024	0.08	0.034	0.056	0.581	0.178
X Czo	0.363	0.356	0.692	0.575	0.564	0.872	0.575	0.587	0.585	0.976	0.893	0.966	0.943	0.418	0.821
X Taw	0.007	0.003	0	0	0.002	0	0.036	0.076	0.011	0	0.027	0	0	0.001	0
X Pist	0.196	0.214	0.104	0.142	0.143	0.042	0.132	0.116	0.132	0.008	0.027	0.01	0.018	0.195	0.059

The formula, expressed in atoms per formula unit, is calculated on the basis of 12.5 atoms of oxygen [X<sub>2</sub>Y<sub>3</sub>Z<sub>2</sub>O<sub>12</sub>(OH)], with Mn<sup>3+</sup>, Mn<sup>2+</sup>, Fe<sup>3+</sup> and Fe<sup>2+</sup> calculated to maximize the occupancy of the Y and X sites. The analyses were done with an electron microprobe. The symbols Taw and Pist refer to "tawmawite" and "pistacite", which are not names of species recognized by the IMA.

13°N + Izu Bonin fore-arc (Alt 1999); diabbases, basalts and gabbros from Holes 1117, 1118, 1109 ODP (Gardien *et al.* 2002)] (Fig. 6b). However, similar high-Mg chlorites have been found in the upper crust of the Hole 736 ODP (forearc basement of Izu-Bonin Arc in the West Pacific; Alt *et al.* 1998). In ophiolites, high-Mg chlorites are relatively uncommon [*e.g.*, East Taiwan (Liou & Ernst 1979), Lizard (Hopkinson & Roberts 1995) and Limousin (Berger *et al.* 2005, J. Berger, pers. commun., 2008)].

#### White mica

Structural formulae are difficult to calculate for micas. In addition to the existence of "true" octahedral vacancies and to the unknown Fe<sup>2+</sup>/Fe<sup>3+</sup> value, also in the case of chlorite, the extent of vacancies in the

twelve-fold site in white micas is uncertain because (1) the mica is generally not analyzed for Ba and Sr, (2) loss of alkalis characterized by a negative "Al-celadonite" end-member (Parra *et al.* 2002) during WDS analyses can occur, and (3) intergrown minerals can be present. This can lead to an overestimation of the extent of vacancies in white micas. Furthermore, incorporation of Ba into the mica structure is facilitated by the presence of chromium (Harlow 1995 in Guidotti & Sassi 1998). The good correlation between 12-fold vacancies and Cr contents for Tisovita-Iuti white micas may thus reflect a high Ba content. In contrast to chlorites, Fe<sup>3+</sup> in micas is known to be controlled by oxygen fugacity conditions (Guidotti *et al.* 1994). The structural formula has been calculated after Vidal & Parra (2000), with Cr<sup>3+</sup> and Fe<sup>3+</sup> incorporated at the [M2 + M3] site. The analyzed Tisovita-Iuti micas are phengitic (Rieder *et al.*

al. 1998), with a composition close to the muscovite end-member (Fig. 7a).

White micas are uncommon in oceanic environments; only biotite is known from gabbros of modern oceanic settings (Stakes *et al.* 1991, Vanko & Stakes 1991, Cannat *et al.* 1997, Robinson *et al.* 2002). Nevertheless, muscovite has been described in ophiolites (Buisson & Leblanc 1987, Ash & Arksey 1990a, b, Lécuyer *et al.* 1990, Halls & Zhao 1995, Berger *et al.* 2005, Nasir *et al.* 2007).

Two groups of white micas can be distinguished in the Tisovita-Iuti rocks on the basis of the  $Fe_{tot}$  contents (Table 6). The first group is characterized by very low Fe content ( $<0.2$  apfu) with  $Fe_{tot} = Fe^{3+}$  according to the

conditions set by Vidal & Parra (2000) and Parra *et al.* (2002) to reject “incorrect” datasets (*i.e.*, compositions that cannot be expressed as a linear combination of the end-members celadonite – muscovite – paragonite – pyrophyllite – biotite). This group of mica compositions is found in clinozoisite-bearing amphibolitized gabbros (Amp-G s2) to listvenites *s.s.* (List s5). The second group is characterized by higher Fe contents (0.2–0.5 apfu) with  $Fe_{tot} = Fe^{2+}$ , and occurs in epidote-bearing amphibolitized gabbros s1 and plagiogranites.

Micas contain higher Cr contents (up to 4.85 wt.%) in the listvenites and the (zoisite + chlorite)-bearing amphibolitized gabbros (Fig. 7b), and consist of chromian phengite. The Cr content is comparable to

TABLE 4. REPRESENTATIVE COMPOSITIONS AND STRUCTURAL FORMULAE OF T-I CHLORITES

Name	Amp-G s2				Czo-G s3			Zo-G s4			List s5				Pl-y	
	Clc-Ame	Clc-Ame	Clc-Dph	Clc-Ame	Clc-Ame	Clc-Ame	Clc-Dph	Clc-Dph	Clc-Ame	Clc-Ame	Ame-Clc	Clc-Ame	Clc-Sud	Clc-Ame	Clc-Dph	Clc-Dph
SiO <sub>2</sub> wt%	28.36	28.53	27.96	28.13	29.05	29.34	29.35	29.44	28.18	29.07	25.12	27.58	28.52	29.15	27.92	27.97
TiO <sub>2</sub>	0.04	0.05	0.05	0.02	0.01	0.01	0.06	0.02	0.03	0.05	0.05	0.20	0.04	0.06	-	0.01
Al <sub>2</sub> O <sub>3</sub>	22.09	22.67	20.96	22.36	21.87	21.20	21.58	20.69	21.49	21.91	20.20	21.23	20.83	21.67	19.35	19.72
Cr <sub>2</sub> O <sub>3</sub>	-	-	0.06	0.28	0.08	0.05	0.05	0.66	0.77	0.46	8.45	4.82	2.87	2.40	-	-
FeO	12.10	9.33	14.78	9.09	9.84	9.92	10.76	11.16	13.06	8.29	10.71	9.03	8.03	6.31	19.97	23.84
MnO	0.19	0.20	0.19	0.11	0.18	0.16	0.20	0.19	0.19	0.11	0.50	2.09	0.13	0.08	0.22	0.33
MgO	24.09	26.18	23.04	26.84	25.55	26.41	25.33	23.85	23.59	26.93	22.20	24.00	23.68	27.31	19.58	16.37
CaO	0.05	0.05	0.08	-	0.08	0.06	0.07	0.12	0.01	0.01	0.04	0.04	0.08	0.04	0.03	0.02
Na <sub>2</sub> O	0.03	-	-	-	-	-	0.05	-	-	0.02	0.02	0.03	-	-	0.02	0.03
K <sub>2</sub> O	0.03	-	0.01	-	0.02	0.02	0.06	0.04	0.01	-	0.06	0.03	0.08	0.03	0.04	0.17
F	-	-	-	-	-	-	-	-	-	-	-	0.11	0.07	0.01	-	-
Cl	0.05	-	-	-	0.01	0.02	0.03	0.01	0.01	0.03	0.03	0.03	0.05	0.02	-	-
Sum	87.03	87.02	87.14	86.83	86.69	87.18	87.55	86.19	87.34	86.88	87.37	87.38	84.38	87.08	87.12	88.46
<sup>71</sup> Si apfu	1.997	1.997	1.997	1.999	1.999	1.999	1.996	1.999	1.998	1.996	1.997	1.986	1.997	1.995	2.000	1.999
<sup>71</sup> Ti	0.003	0.003	0.003	0.001	0.001	0.001	0.004	0.001	0.002	0.004	0.003	0.014	0.003	0.005	-	0.001
<sup>72</sup> Si	0.798	0.773	0.799	0.738	0.838	0.852	0.859	0.918	0.789	0.817	0.542	0.728	0.866	0.807	0.872	0.892
<sup>72</sup> Al	1.202	1.227	1.201	1.262	1.162	1.148	1.141	1.082	1.211	1.183	1.458	1.272	1.134	1.193	1.128	1.108
<sup>M4</sup> Al	1.000	1.000	0.995	0.979	0.994	0.996	0.996	0.949	0.940	0.965	0.325	0.625	0.772	0.817	1.000	1.000
<sup>M4</sup> Cr	-	-	0.005	0.021	0.006	0.004	0.004	0.051	0.060	0.035	6.775	3.375	0.228	0.183	-	-
<sup>M4</sup> Al	0.202	0.227	0.201	0.262	0.162	0.148	0.141	0.082	0.211	0.183	0.458	0.272	0.134	0.193	0.128	0.108
<sup>M1</sup> Mg	0.547	0.572	0.549	0.586	0.595	0.637	0.601	0.594	0.535	0.617	0.328	0.460	0.540	0.597	0.514	0.424
<sup>M1</sup> Fe	0.154	0.114	0.197	0.111	0.128	0.134	0.143	0.156	0.166	0.107	0.089	0.097	0.103	0.077	0.294	0.346
<sup>M1</sup> Mn	0.016	0.017	0.016	0.009	0.015	0.013	0.017	0.016	0.016	0.009	0.043	0.024	0.011	0.006	0.019	0.029
<sup>M1</sup> □	0.081	0.070	0.037	0.032	0.100	0.069	0.098	0.151	0.072	0.084	0.083	0.147	0.212	0.126	0.045	0.093
<sup>M2+M3</sup> Al	0.163	0.140	0.075	0.063	0.200	0.137	0.196	0.303	0.144	0.168	0.166	0.293	0.425	0.253	0.089	0.186
<sup>M2+M3</sup> Mg	2.993	3.217	2.886	3.308	3.125	3.190	3.072	2.929	2.942	3.267	3.017	3.060	3.004	3.317	2.488	2.099
<sup>M2+M3</sup> Fe	0.844	0.643	1.039	0.629	0.675	0.672	0.732	0.768	0.914	0.564	0.816	0.646	0.571	0.430	1.423	1.715
Mg#	0.780	0.833	0.735	0.840	0.822	0.826	0.808	0.792	0.763	0.853	0.787	0.826	0.840	0.885	0.636	0.550
X Clc	0.559	0.586	0.560	0.594	0.607	0.647	0.615	0.607	0.547	0.625	0.362	0.480	0.549	0.603	0.526	0.439
X Dph	0.158	0.117	0.202	0.113	0.131	0.136	0.146	0.159	0.170	0.108	0.098	0.101	0.104	0.078	0.301	0.359
X Sud	0.081	0.070	0.037	0.032	0.100	0.069	0.098	0.151	0.072	0.084	0.083	0.147	0.212	0.126	0.045	0.093
X Ame	0.202	0.227	0.201	0.262	0.162	0.148	0.141	0.082	0.211	0.183	0.458	0.272	0.134	0.193	0.128	0.108

The formula, expressed in atoms per formula unit, is calculated on the basis of 14 atoms of oxygen, with sites occupancies following Vidal & Parra (2000) and  $Fe_{total} = Fe^{2+}$ ;  $Mg\# = Mg/(Mg + Fe_{total})$ . The analyses were done with an electron microprobe. See Table 5 for a comment about end members in the chlorite group of minerals.

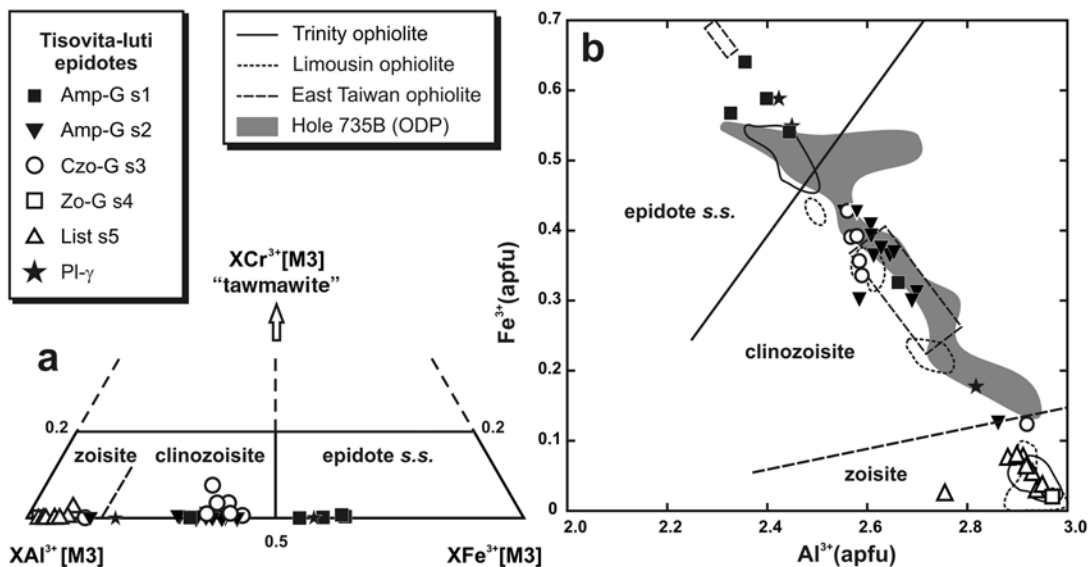


FIG. 5. a. Classification of Tisovita–luti epidote-group minerals in a triangular diagram based on the  $X[M3]$  content (adapted from Franz & Liebscher 2004) :  $XFe^{3+} = Fe^{3+}/(Fe^{3+} + Al^{3+} - 2 + Cr^{3+})$ ,  $XCr^{3+} = Cr^{3+}/(Fe^{3+} + Al^{3+} - 2 + Cr^{3+})$ ,  $XAl^{3+} = (Al^{3+} - 2)/(Fe^{3+} + Al^{3+} - 2 + Cr^{3+})$ . b. Comparison between Tisovita–luti epidote-group minerals and ancient and modern oceanic occurrences. Compilation from 1 and 4 (see caption of Fig. 4), 5: Limousin ophiolite, France (metagabbros) (Berger *et al.* 2005 and pers. commun., 2008), 6: East Taiwan ophiolite, Taiwan (gabbros, veins in gabbros, rodingites) (Liou & Ernst 1979). “Tawmawite” (*i.e.*, Cr-rich epidote) is shown in quotation marks because it is not an IMA-approved name.

other compositions of chromian mica in the literature (Whitmore *et al.* 1946). Moreover, these micas are similar to those described in others ophiolite-associated occurrences of listvenite (Buisson & Leblanc 1987, Ash & Arksey 1990a, b, Halls & Zhao 1995, Nasir *et al.* 2007).

#### GEO THERMOMETRY

The Tisovita–luti listvenites (*i.e.*, List s5) contain the association zoisite + chlorite + phengite. Zoisite occurs typically in low-pressure metasomatic assemblages by the breakdown of plagioclase (*e.g.*, Klemd 2004). A tentative multi-equilibria approach on the mineral pair chlorite–phengite (Vidal & Parra 2000) was first investigated to constrain the temperature and pressure of listvenite formation. Results display well-constrained temperatures, whereas pressure estimation is not achievable. Consequently, geothermometric conditions of formation of these low-pressure metasomatic lithologies were determined using a thermodynamic model based solely on the compositions of chlorite (Vidal & Parra 2000, Vidal *et al.* 2001, 2005, 2006). Empirical geothermometers based on chlorite (Cathelineau 1988, Kranidiotis & MacLean 1987, Jowett 1991, Hillier & Velde 1991, Zang & Fyfe 1995) were applied on the Tisovita–luti chlorites (Fig. 8a) for comparison with

TABLE 5. NAMES AND FORMULAE OF CHLORITE END-MEMBERS USED IN THIS INVESTIGATION

Chlorite end-member	Formula
clinocllore (Clc)	$Mg_2Al(Si_4Al)O_{10}(OH)_2$
daphnite (Daph)	$Fe_2Al(Si_4Al)O_{10}(OH)_2$
Mg-amesite (Mg-Ame)	$Mg_2Al_2(Si_2Al_2)O_{10}(OH)_2$
Fe-amesite (Fe-Ame)	$Fe_2Al_2(Si_2Al_2)O_{10}(OH)_2$
Mg-sudoite (Mg-Sud)	$Mg_2Al_2(Si_4Al)O_{10}(OH)_2$

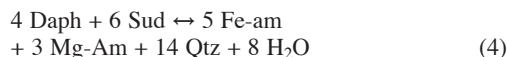
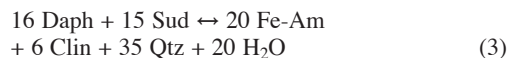
The nomenclature used here follows the thermodynamic approach of Vidal & Parra (2000), Vidal *et al.* (2001, 2005). Note that the clinocllore end-member as defined here has a different composition than what is defined by the IMA, but it seems a more realistic representation of clinocllore compositions in general. The other names of end members are not recognized by the IMA or contravene a rule of nomenclature of the IMA.

the thermodynamic approach. The geobarometric conditions were estimated with the empirical P–T relation of Velde (1967) based on the Si content in micas.

#### Thermodynamic model to estimate the temperature of equilibration

The internally consistent WINTWQ software (version 2.32) based on a multi-equilibrium calculation (Berman 1991) was used in association with the thermodynamic database on chlorite end-members of Vidal *et al.*

(2001). Following Vidal & Parra (2000), four equilibrium reactions (Eq. 1–4) using five end-members of chlorite-group minerals proposed by those authors [clinocllore (Clc), Fe-amesite (Fe-Am), Mg-amesite (Mg-Am), daphnite (Daph) and Mg-sudoite (Mg-Sud)] can be used:



These reactions define four geothermometric curves in a P–T grid. Reaction (2) is very sensitive to small compositional changes, and the curve generated is generally outside the stability field of chlorite. Consequently, the average temperature was calculated only on the three other reactions (invariably close to each other, in a range of 80°C) for a pressure fixed at 2.5 kbar. Forty-two compositions of Tisovita–Iuti chlorite conform to the conditions defined by Vidal & Parra (2000) and Vidal *et al.* (2001); they can be expressed as a linear combination of the five end-members. For some samples, the three curves are not strictly T-dependent and were adjusted assuming  $\text{Fe}^{3+} = 0.15 \times \text{Fe}_{\text{tot}}$ , the maximum  $\text{Fe}^{3+}$  content of chlorites according to Dyar *et al.* (1992).

In contrast with the results of empirical thermometry (Fig. 8a), the frequency distributions of T estimated by this thermodynamic model are more complex and extend over a larger range of temperatures (Fig. 8b). In all rock types except Amp–Gs 2, which displays relatively high temperatures (~450°C), two distinct populations of chlorite can be distinguished: a group of low-T chlorites (280–320°C) that is quite comparable to the results obtained with empirical thermometers (Fig. 8a), and a group of higher-T chlorites (400–460°C). This bimodal distribution of temperature is not related to the Cr content of chlorite, but is consistent with petrological observations. Indeed, high-T chlorites occur as large tabular crystals (Fig. 3b) or as the core of the smaller grains, whereas low-T chlorites are found in microcrystalline association with the micas (Fig. 3d), as a rim on high-T chlorites, or in replacement of actinolite. A pressure estimate of less than 4 kbar is proposed for  $T \leq 400^\circ\text{C}$  using the P–T relation of Velde based on the Si content in micas (3.1 to 3.3 apfu for T–I micas).

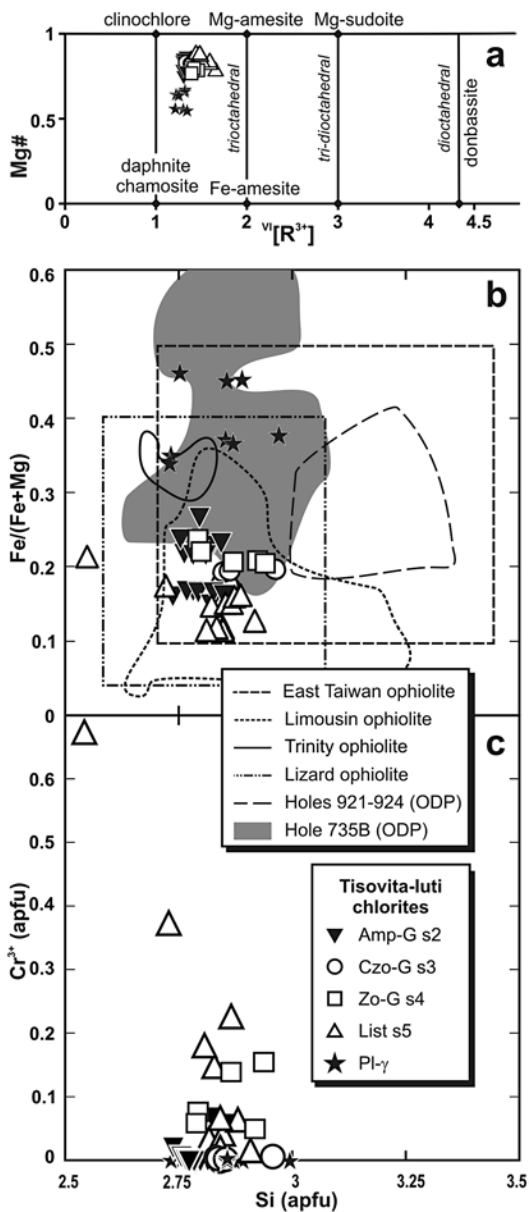


FIG. 6. (a) Classification of Tisovita–Iuti chlorite-group minerals showing the high  $\text{Mg}\# = \text{Mg}/(\text{Mg} + \text{Fe}_{\text{tot}})$  in gabbro-derived rocks. (b) Composition of Tisovita–Iuti chlorites and comparison with ancient and modern oceanic occurrences (after Nimis *et al.* 2004). Compilation from 1, 2, 3 and 4 (see caption of Fig. 4), 5 and 6 (see caption of Fig. 5). (c) Cr contents found in the Tisovita–Iuti chlorites. See Table 5 for a comment on the nomenclature of chlorite-group minerals.

TABLE 6. REPRESENTATIVE COMPOSITIONS AND STRUCTURAL FORMULAE OF T-J PHENGITE

Name	Amp-G s1			Amp-G s2			Czo-G s3			Zo-G s4			List s5			Pl-y		
	Phg	Phg	Phg	Phg	Phg	Phg	Phg	Phg	Phg	Phg	Phg	Phg	Phg	Phg	Phg	Phg	Phg	
SiO <sub>2</sub> wt%	48.22	49.07	48.14	47.45	49.50	49.17	49.74	50.57	50.53	50.18	47.83	47.45	45.37	49.23	47.42	47.75	47.78	46.30
TiO <sub>2</sub>	0.19	0.08	0.17	0.43	0.15	0.30	0.27	0.28	0.22	0.24	0.51	0.35	0.37	0.42	0.43	0.33	-	0.27
Al <sub>2</sub> O <sub>3</sub>	32.94	32.01	32.58	32.66	32.11	30.64	30.88	31.07	28.12	29.42	34.24	31.84	30.05	30.49	33.31	30.41	31.42	30.27
Cr <sub>2</sub> O <sub>3</sub>	-	0.00	0.22	0.05	0.02	0.89	0.48	0.12	3.53	1.20	0.41	3.19	4.85	4.09	1.06	4.02	0.05	-
FeO	2.41	0.85	0.96	1.29	1.15	1.29	1.34	1.41	1.12	1.27	0.63	0.62	1.47	0.98	0.99	1.15	2.41	3.75
MnO	-	-	-	0.02	-	0.02	-	0.01	0.02	-	-	-	-	-	0.03	-	-	0.05
MgO	1.71	2.23	2.04	1.97	2.54	2.67	2.58	2.88	3.04	2.97	1.62	1.68	3.04	2.35	1.79	2.32	1.84	2.13
CaO	0.09	0.04	-	-	0.01	-	0.02	0.09	-	0.01	0.02	-	-	0.03	0.02	0.03	0.18	-
Na <sub>2</sub> O	0.86	0.89	1.13	0.48	0.42	0.31	0.28	0.33	0.23	0.26	0.50	0.61	0.52	0.42	0.70	0.51	0.89	0.32
K <sub>2</sub> O	8.00	8.70	8.39	8.63	9.29	8.80	7.90	8.45	6.78	8.66	9.04	7.83	7.80	5.85	8.66	8.05	7.80	9.19
F	0.06	-	-	0.02	-	0.10	0.13	-	0.02	0.06	-	-	0.03	0.08	0.07	0.05	-	-
Cl	-	-	-	0.01	-	-	-	0.02	0.01	0.01	0.01	-	0.01	0.01	0.03	0.01	-	-
Sum	94.47	93.88	93.64	92.98	95.18	94.17	93.62	95.22	93.61	94.27	94.79	93.58	93.50	93.95	94.50	94.62	92.37	92.28
<sup>71</sup> Si	2	2	2	2	2	2	2	2	2	2	2	2	2	2	2	2	2	2
<sup>72</sup> Si	1.204	1.258	1.207	1.185	1.249	1.268	1.298	1.301	1.353	1.326	1.152	1.175	1.080	1.248	1.146	1.182	1.245	1.202
<sup>72</sup> Al	0.796	0.742	0.793	0.815	0.751	0.732	0.702	0.699	0.647	0.674	0.848	0.825	0.920	0.752	0.854	0.818	0.755	0.798
<sup>71</sup> Ti	0.010	0.004	0.009	0.022	0.007	0.015	0.014	0.014	0.011	0.012	0.025	0.018	0.019	0.021	0.022	0.017	0.000	0.014
<sup>M2+M3</sup> Al	1.783	1.762	1.766	1.769	1.733	1.667	1.711	1.692	1.552	1.624	1.812	1.686	1.485	1.618	1.751	1.570	1.760	1.670
<sup>M2+M3</sup> Cr	-	-	0.01	-	-	0.05	0.03	0.01	0.18	0.06	0.02	0.17	0.26	0.21	0.06	0.21	-	-
<sup>M2+M3</sup> Fe <sup>3+</sup>	-	0.047	0.054	0.072	0.063	0.072	0.074	0.077	0.062	0.070	0.035	0.035	0.083	0.054	0.055	0.064	-	-
<sup>M2+M3</sup> Mg	0.121	0.191	0.169	0.156	0.202	0.214	0.190	0.225	0.201	0.242	0.132	0.110	0.172	0.115	0.138	0.154	0.137	0.166
<sup>M2+M3</sup> Fe <sup>2+</sup>	0.096	-	-	-	-	-	-	-	-	-	-	-	-	-	-	-	-	-
<sup>M1</sup> Mg	0.048	0.030	0.034	0.041	0.046	0.050	0.066	0.055	0.099	0.050	0.026	0.058	0.136	0.116	0.038	0.076	0.050	0.053
<sup>M1</sup> Fe <sup>2+</sup>	0.038	-	-	-	-	-	-	-	-	-	-	-	-	-	-	-	0.037	0.053
<sup>M1</sup> □	0.913	0.970	0.966	0.959	0.954	0.949	0.934	0.945	0.900	0.950	0.974	0.942	0.864	0.884	0.960	0.924	0.914	0.891
<sup>A</sup> K	0.678	0.737	0.713	0.739	0.778	0.746	0.668	0.704	0.573	0.732	0.760	0.668	0.676	0.492	0.733	0.684	0.676	0.811
<sup>A</sup> Na	0.111	0.115	0.146	0.062	0.053	0.040	0.035	0.042	0.030	0.034	0.064	0.079	0.069	0.054	0.090	0.066	0.118	0.043
<sup>A</sup> □	0.205	0.146	0.141	0.199	0.169	0.214	0.295	0.248	0.397	0.234	0.175	0.253	0.255	0.452	0.176	0.248	0.194	0.146

Mg#	0.56	0.82	0.79	0.73	0.80	0.79	0.77	0.78	0.83	0.81	0.82	0.83	0.79	0.81	0.76	0.78	0.58	0.50
X <sub>Ms</sub>	0.59	0.61	0.62	0.67	0.65	0.62	0.58	0.58	0.47	0.57	0.71	0.60	0.54	0.37	0.68	0.60	0.56	0.63
X <sub>Pri</sub>	0.10	0.09	0.13	0.06	0.04	0.03	0.03	0.03	0.02	0.03	0.06	0.07	0.05	0.04	0.08	0.06	0.10	0.03
X <sub>Bt</sub>	0.21	0.15	0.14	0.20	0.17	0.21	0.30	0.25	0.40	0.23	0.17	0.25	0.26	0.45	0.18	0.25	0.19	0.15
X <sub>Alcel</sub>	0.10	0.03	0.04	0.06	0.05	0.07	0.08	0.07	0.11	0.06	0.05	0.08	0.15	0.14	0.06	0.09	0.09	0.12
X <sub>Pg</sub>	0.01	0.12	0.08	0.01	0.09	0.07	0.02	0.07	0.00	0.11	0.00	0.00	0.00	0.00	0.00	0.00	0.06	0.07

The formula, expressed in atoms per formula unit, is calculated on the basis of 22 atoms of oxygen, with sites occupancies following Vidal & Parra (2000). Note that  $Fe_{\text{total}} = Fe^{3+}$  for Amp-G s2, Czo-G s3, Zo-G s4 and List s5;  $Fe_{\text{total}} = Fe^{2+} + Fe^{3+}$  for Amp-G s1 and Pl-Y;  $Mg\# = Mg/(Mg + Fe_{\text{total}})$ . The analyses were done with an electron microprobe.

## DISCUSSION

### *Chlorite–phengite equilibria and the listvenitic paragenesis*

Several mineral assemblages have been observed and described in the variously transformed Tisovita–Iuti gabbros. Phengite and chlorite occur together in all of them, however, and their relative modal proportions increase with the degree of metasomatic changes. Textural equilibrium between these two phases has already been suggested by petrographic observations made of the listvenites (List s5), where they occur in a close microcrystalline association. This is confirmed by using the chemical composition of chl–phg pairs for each lithology: the tie-lines for all analyzed pairs are parallel in an  $^{IV}Al - (^{VI}Al + Cr + Fe^{3+})$  diagram (Fig. 9a), which illustrates the similar behavior of these phases during metasomatic evolution. This equilibrium is also suggested by the correlation for each pair between the Mg# of chlorite and phengite (Fig. 9b). Furthermore, the high Cr contents are observed for both chlorite (Fig. 6c) and phengite (Fig. 7b) in the same lithologies (List s5 and Zo–G s4). Consequently, the P–T conditions of formation of phengite are quite comparable to those of chlorite. More precisely, according to their similar habit, the crystallization of unusual chromian phengite can be discussed in terms of results on the low-temperature chlorite to constrain the complete paragenesis of the listvenites (zoisite – chlorite – phengite – calcite).

### *Thermometry results*

De Caritat *et al.* (1993) have shown that the empirical thermometers based on chlorite do not yield satisfactory results over the whole range of natural conditions. Indeed, chemical compositions of chlorite depend not only on temperature, but also on bulk-rock composition, fluid composition,  $f(O_2)$ , *etc.* Zane *et al.* (1998) concluded that chlorite composition is mainly controlled by the bulk-rock composition, obscuring the changes caused by P and T. Moreover, empirical geothermometers were calibrated with chlorites displaying high contents of Fe [ $Fe/(Fe + Mg)$  in the range 0.24–0.85] in contrast to those of Tisovita–Iuti gabbro-derived lithologies [ $Fe/(Fe + Mg)$  in the range 0.11–0.23]. Nevertheless, the temperatures obtained by the thermodynamic approach display different results (two populations and higher T) that are more consistent with petrographic observations and variations in chlorite composition (Fig. 10) and can be interpreted in terms of processes at different temperatures. The divergence of results between the empirical and thermodynamic approaches at high temperatures ( $\geq 400^\circ C$ ) was already highlighted by Vidal *et al.* (2006), who have shown that at high temperature, different estimates of temperature can be obtained for the same  $^{IV}Al$  content. In contrast

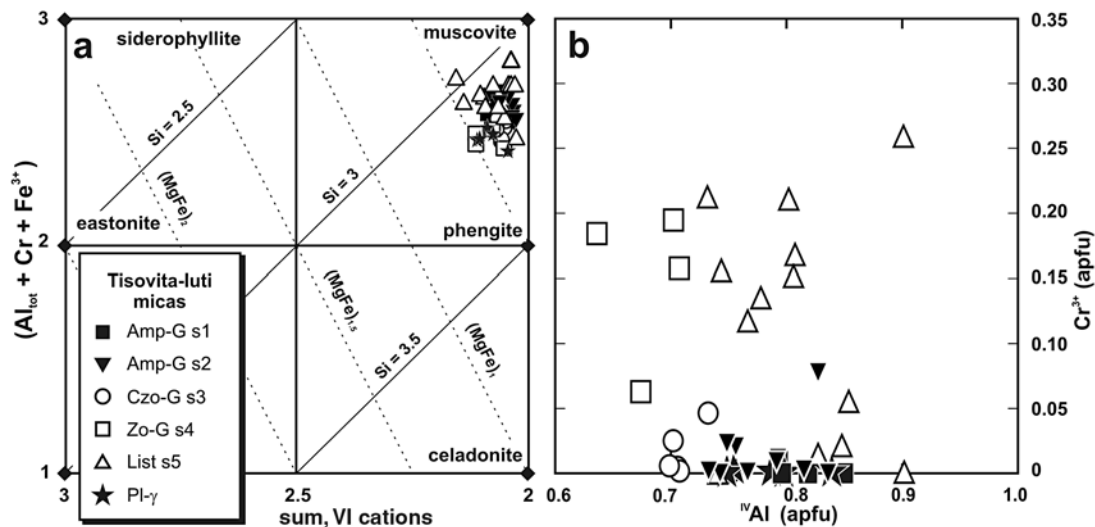


FIG. 7. (a) Classification of Tisovita-Iuti micas; (b) Cr contents found in the Tisovita-Iuti white micas.

to empirical relations, temperatures appear to be linked to the global composition of chlorite illustrated by the “Al-chl” parameter (Fig. 10) of de Caritat *et al.* (1993). The Tisovita-Iuti chlorites, although of a limited range of composition, display the same behavior in conjunction with temperatures obtained with TWQ (Fig. 10). Consequently, as the empirical relations are not valid at high temperatures, thermometric interpretations were made with the thermodynamic results only.

The two distinct populations of chlorite (Low-T and High-T) correspond to two distinct habits of the chlorite grains: the large tabular crystals and the microcrystalline association with the micas. The chlorite populations are used to define two distinct thermal events in the geological history: 1) a medium-T stage (~450°C) that occurred during the high-T chlorite – epidote – clinozoisite – actinolite – albite crystallization (hydrothermal metamorphism), and 2) a low-T stage (~300°C) that partially (s1, s2, s3) or totally (s4, s5) replaced the former association and gave rise to the chlorite – phengite – zoisite – calcite assemblage (metasomatism). The two-stage evolution is not related to the Cr content of chlorite; nevertheless, the Cr content of both mica and chlorite increases dramatically (*i.e.*, Cr is not removed) with progress of the low-T metasomatic process.

#### Origin of the chromium enrichment

The origin of the chromium in listvenite directly depends on 1) the primary mineral acting as a source and its ability to release chromium and 2) the behavior of Cr during fluid-linked metasomatism. In an ultra-

mafic or mafic environment, chromite is the primary source of chromium, which occurs as Cr<sup>3+</sup>. However, chromium is not easily released from chromite, even under high-temperature conditions. The destabilization of chromite during hydrothermal alteration is a well-known process that generally leads to the formation of a rim of Cr-Fe<sup>3+</sup>-enriched spinel or Cr-rich magnetite around a relict preserved core, and that promotes the formation of chlorite aureoles (Shen *et al.* 1988, Kimball 1990, Mellini *et al.* 2005). The retention of Cr<sup>3+</sup> in chromite is linked to his high octahedral site-preference energy (OSPE), which predicts that Cr<sup>3+</sup> will be the last ion to be removed from the spinel structure (Oze 2003). However, in some cases, a small-scale diffusion of Cr out of the spinel is found, and Cr is directly enclosed in the surrounding silicates (Hamlyn 1975, Mussallam *et al.* 1981, Mitra *et al.* 1992, Halls & Zhao 1995, Graham *et al.* 1996, Abzalov 1998, Oze 2003). Extensive release of Cr from chromite is only seen in particular conditions: Cr<sup>3+</sup> diffusion under high-P and low-T conditions (Mével & Kienast 1980) or dissolution of chromite and subsequent release of Cr under highly oxidizing conditions, such as in the presence of Mn oxides (Oze 2003).

In the Tisovita-Iuti gabbros, some spinel compositions [*e.g.*, (Mg<sub>0.47</sub>Fe<sub>0.50</sub>) (Al<sub>1.34</sub>Cr<sub>0.50</sub>Fe<sub>0.15</sub>) O<sub>4</sub>] are destabilized in the common way described above, and chromium is mobilized only at the scale of mm into the surrounding chlorite grains (Fig. 3e). Spinel destabilization could be related to reaction with 1) a fluid enriched in Mg and Si during a high-T metasomatism (T > 400°C), following equations 5 and 6 of Kimball (1990) and Mellini *et al.* (2005), respectively:



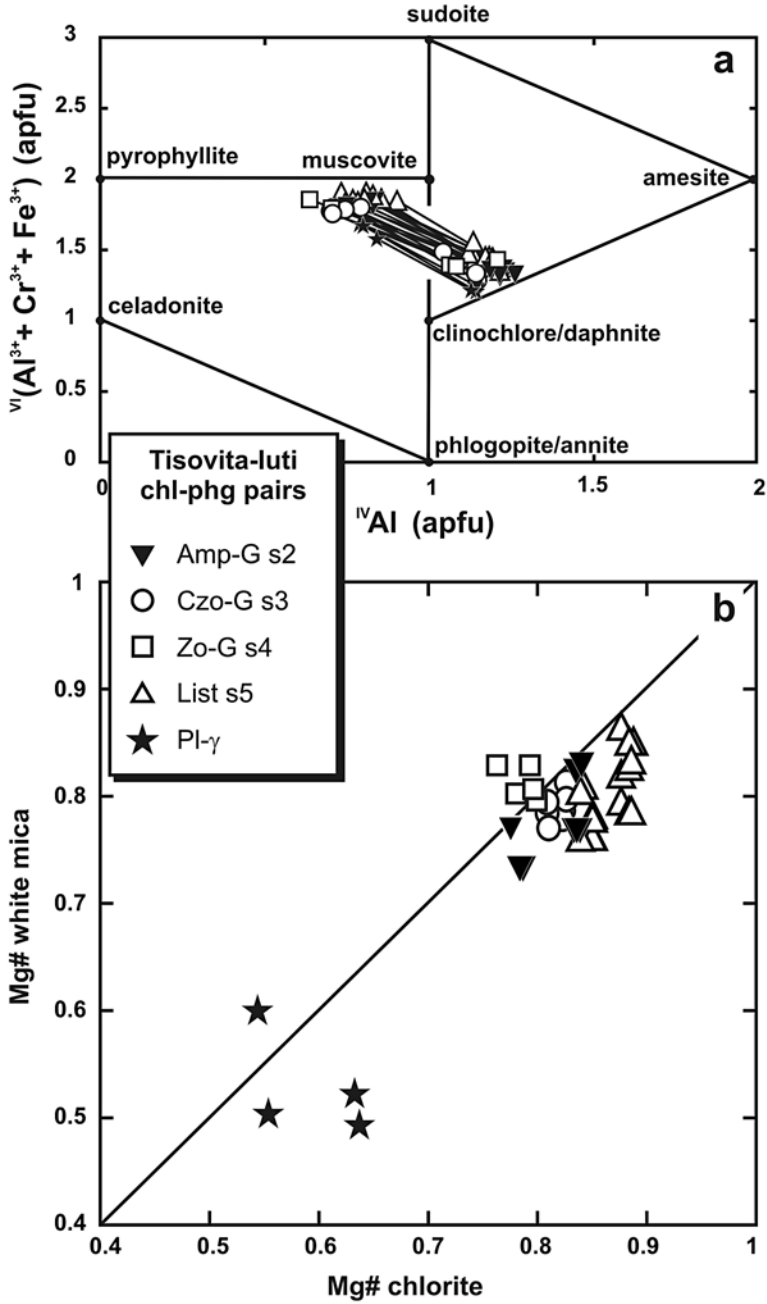


FIG. 9. Chlorite–phengite equilibria. (a) Parallelism between tie-lines joining of chlorite–phengite pairs. (b) Correlation of Mg# of chlorites and phengites.

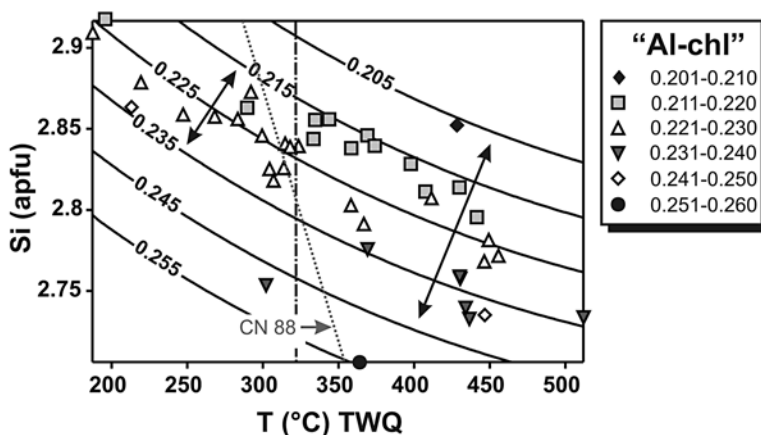
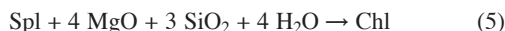


FIG. 10. Distribution of Tisovita–Iuti chlorites  $^{19}\text{Si}$  (apfu) versus TWQ-derived temperature showing several trends of decreasing Si with T depending of the “Al-chl” parameter defined by de Caritat *et al.* (1993) as:  $\text{Al-chl} = \text{Al}_{\text{tot}} / (\text{Al}_{\text{tot}} + 2 \text{Fe}^{2+} + 2 \text{Mg})$  and adapted here for Cr-bearing chlorite as:  $\text{Al-chl} = (\text{Al}_{\text{tot}} + \text{Cr}^{3+} + \text{Fe}^{3+}) / (\text{Al}_{\text{tot}} + \text{Cr}^{3+} + \text{Fe}^{3+} + 2 \text{Fe}^{2+} + 2 \text{Mg})$ . The Si content classically decreases with T in low-T chlorites, but this trend is more T-dependent (flat profile) than classical empirical T–Si relations [*i.e.*, Cathelineau & Nieva (1985), CN88], which allows us to obtain high-T results.



with possible diffusion of Cr between spinel and chlorite, or 2) a Mg-rich silicate (olivine) and  $\text{H}_2\text{O}$ , as expressed by equation 7:



Chromium is thus first locally transferred into silicates (local aureole of chromian chlorite, Fig. 3e) during the destabilization of the spinel associated with a high-T metasomatic event prior to the formation of listvenite. During a subsequent stage of alteration,  $\text{Cr}^{3+}$  can be more easily leached from silicates. However,  $\text{Cr}^{3+}$  is known to be a chemically immobile cation in fluids owing to the formation of highly stable (oxy)hydroxides; on the contrary,  $\text{Cr}^{6+}$  forms soluble anions (Burke *et al.* 1991, Ball & Nordstrom 1998). Oxidation of  $\text{Cr}^{3+}$  to  $\text{Cr}^{6+}$  by oxygen in seawater is extremely slow (Van der Weijden & Reith 1982), and the only important pathway for oxidation in natural systems is probably oxidation by Mn oxides (Fendorf 1995, Oze 2003). The mobilization of  $\text{Cr}^{3+}$  is, however, seen in shear zones (Winchester & Max 1984), with strongly acidic conditions ( $\text{pH} < 4$ ) (Oze 2003) and in special systems such as Outokumpu, Finland (Treloar 1987). All the conditions mentioned above do not fit with the environment of formation of the listvenite of Tisovita–Iuti. Conse-

quently, even if small amounts of  $\text{Cr}^{3+}$  are leached from the Cr-rich silicates during listvenite formation, they are not transformed into  $\text{Cr}^{6+}$  and cannot be mobilized. Chromium, as aluminum, is thus considered as immobile or only slightly mobilized (mm scale, see Fig. 3e) during listvenite formation. In the same way, the early Cr-rich chlorite exchanges its Cr with the new low-T silicates to form the Cr-rich low-T chlorite – phengite – zoisite – calcite assemblage. Consequently, if no chromite is present in the rock as a primary source of Cr, we observe Cr-free phengite and low-T Cr-free chlorite in equilibrium with calcite and zoisite.

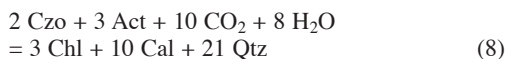
#### Ocean-floor metamorphism

The gabbros of the Tisovita–Iuti ophiolite illustrate a complex transformation history in several stages, after their magmatic crystallization. The first event of transformation corresponds to hydrothermal metamorphism, ranging from the amphibolite to the greenschist facies.

The Eastern gabbros of the Tisovita–Iuti ophiolite are converted to amphibolite on a regional scale, this process being commonly observed in ophiolites (Mével *et al.* 1978, Girardeau & Mével 1982, Lécuyer *et al.* 1990, Hopkinson & Roberts 1995, Berger *et al.* 2005). The primary clinopyroxene and plagioclase react with  $\text{H}_2\text{O}$  to give amphibole and a more sodic plagioclase ( $\text{An}_{0-12}$  in sample Amp-G s1). Circulation of seawater-derived fluids can hydrate the mafic lithologies as they cool and during frequent plastic deformation,

which characterize slow-spreading ridge environments (Mével 1988, Stakes *et al.* 1991, Vanko & Stakes 1991, Cannat *et al.* 1991, 1997, Dilek *et al.* 1997, Talbi *et al.* 1999, Robinson *et al.* 2002). This retrograde H<sub>2</sub>O-rich metamorphism is typical of ocean-floor processes, also observed in the Tisovita–Iuti ophiolite.

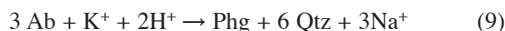
A second stage of the retrograde metamorphism occurs at the amphibolite–greenschist facies transition, which generates the association actinolite – sodic plagioclase – clinozoisite – high-T chlorite – titanite (samples Amp–G s2 and Czo–G s3). The content of Fe<sup>3+</sup> in epidote-group minerals is related to their formation from amphibole and not from plagioclase (Franz & Liebscher 2004). Calcite can form during this metamorphic event by replacement of amphibole following reaction 8 (Kishida & Kerrich 1987).



Similar greenschist assemblages are known in ophiolites (Liou & Ernst 1979, Lécuyer *et al.* 1990, Hopkinson & Roberts 1995, Berger *et al.* 2005) and in modern oceanic environments (Mével 1988, Fletcher *et al.* 1997, Stakes *et al.* 1991, Vanko & Stakes 1991, Cannat *et al.* 1991, 1997, Talbi *et al.* 1999, Robinson *et al.* 2002). According to our geothermometric results based on chlorite, this stage occurs at moderate temperature (~450°C), in agreement with experimental studies (Liou *et al.* 1974).

#### Listvenite formation

The process of listvenite formation occurs at lower temperatures than 450°C and partially or totally replaces the previous amphibolite and medium-temperature greenschist paragenesis. Low-pressure and low-temperature conditions obtained using mica compositions and chlorite geothermometry are in agreement with those estimated at 270–390°C and 1–3 kbar at others occurrences (*e.g.*, Halls & Zhao 1995, and references therein) and those (200 < T < 400°C, 2 < pH < 4) for beresite formation (Zharikov *et al.* 2007). In Amp–G s1 to Amp–G s3 assemblages, listvenite formation is not achieved. Instead, there is only the development of phengite and low-T chlorite as a rim on high-T chlorite or as a replacement of actinolite. Low-T chlorite is more magnesian than high-T chlorite. This high content of Mg reflects the leaching of Fe from the rocks during the more intense metasomatic event. According to Kishida & Kerrich (1987), phengite can form from albite according to reaction 9:



Phengite could reflect a uniquely K-rich metasomatism (Eq. 9) where there is no evidence for strong *f*(CO<sub>2</sub>) (*i.e.*, in stages Amp–G s1 to Czo–G s3). Such K<sup>+</sup> enrich-

ment has been observed in gabbros of Hole 735B and interpreted as an oceanic late-stage low-T alteration (Bach *et al.* 2001).

The complete process of listvenite formation leads to a zoisite – chlorite – phengite – calcite assemblage (samples Zo–Gs 4 and List s 5). The high Al content of zoisite is directly linked to the breakdown of plagioclase. A low Fe content can also correspond to intense metasomatism that leaches iron from the rocks. At this stage, amphibole is completely replaced by chlorite, and plagioclase is transformed to zoisite under low *f*(CO<sub>2</sub>) following reaction 10 (Klemd 2004).



Calcite forms under higher *f*(CO<sub>2</sub>) and can be generated from zoisite following the reverse of reaction 10. Calcite is also present in veinlets and can be interpreted as a late phase. The presence of calcite with zoisite involves variations in the CO<sub>2</sub> content of the fluid or an interaction with another fluid richer in CO<sub>2</sub>. A similar equilibrium between calcite and clinozoisite is seen in hydrothermally altered greenstone complex of Archean age (Kitajima *et al.* 2001). It is directly dependent on the variations of *f*(CO<sub>2</sub>) in the seawater-derived fluids due to a phase separation during the ascending path. In contrast to the Tisovita–Iuti classical listvenites derived from an ultramafic precursor (*i.e.*, carbonate-rich), the predominance of zoisite on calcite in gabbro-derived listvenites indicates a fluid very poor in CO<sub>2</sub> (*X* ≈ 0.05 according to Storre & Nitsch 1972), which can correspond to bottom seawater (2.38 mmol/kg CO<sub>2</sub>, according to Craig *et al.* 1981).

#### Geotectonic environment of listvenite formation

Listvenites from Tisovita–Iuti are widespread and originated from different types of rocks (mafic, ultramafic, silicic). During hydrothermal activity at the ridge axis, K<sup>+</sup> from seawater-derived fluids is integrated into micas or clay minerals in the uppermost part of the oceanic crust (*i.e.*, basalts) (Alt & Honnorez 1984, Honnorez 2003) or deep lithologies (gabbro and serpentinite) exposed along detachment faults (*i.e.*, Hole 735B, after Bach *et al.* 2001). Present-day detachment faults in oceanic settings (*e.g.*, Dick *et al.* 1991, Karson & Lawrence 1997, Escartin *et al.* 2003, Searle & Escartin 2004, Canales *et al.* 2004, Boschi *et al.* 2006a) display common talc – amphibole – chlorite – serpentine schists (see Boschi *et al.* 2006b for a review) and more rarely amphibole–carbonate schists (Schroeder & John 2004). However, carbonate-rich serpentinite breccias (ophicalcites) are known to be in some cases related to oceanic detachment faults (Treves & Harper 1994), generated in the final unroofing of the serpentinized upper mantle. These ophicalcite-bearing detachment faults pertain to the ocean–continent transition (*e.g.*, Lemoine *et al.* 1987, Manatschal & Muntener 2008) and mid-ocean

ridge setting (e.g., Escartin *et al.* 2003). In both cases, carbonatization is linked to the calcareous sediments occurring near the detachment fault (Hopkinson *et al.* 2004). Regarding the localization of the listvenites inside the ophiolitic massifs (Fig. 1), gabbro-derived listvenites appear distinctly restricted to the Eastern part of each massif. This particular alignment could reflect an ancient discontinuity (detachment fault?), certainly a factor in localizing obduction and post-collisional tectonics.

### CONCLUSIONS

The gabbros of the Eastern part of the Tisovita–Iuti ophiolite, in Romania, have been affected by a strong alteration, which occurred as two distinct moderate-temperature and low-temperature events. The first event corresponds to a large-scale gradual retrograde ocean-floor metamorphism of the gabbroic protolith (Amp–Gs 1 to Czo–G s3), and the second is characterized by the local metasomatic transformation of previous lithologies to listvenite (Zo–G s4 to List s5). Although the formation of listvenite is in some cases attributed to post-obduction metasomatism linked to deuteritic fluids derived from a granitic intrusion, such a metasomatism is neither recorded in the Tisovita–Iuti ophiolite nor in its host rocks. Phengite and chlorite are common in the listvenite assemblages and are interpreted as late but real oceanic-floor-related phases. Chromian phengite in the Tisovita–Iuti listvenites has certainly formed in an oceanic environment soon after the main ocean-floor metamorphism. Low-pressure and low-temperature conditions obtained by mica compositions and chlorite thermometry could reflect the reaction of seawater with exhumed amphibolitized gabbros along possible detachment faults in an oceanic setting.

### ACKNOWLEDGEMENTS

The authors are grateful to P.T. Robinson and an anonymous reviewer for their helpful comments and suggestions. This work benefitted from the editorial help and comments of R.F. Martin and T. Grammatikopoulos. This study was done in the framework of a Romania – Wallonie – Bruxelles cooperation.

### REFERENCES

- ABZALOV, M.Z. (1998): Chrome-spinels in gabbro–wehrlite intrusions of the Pechenga area, Kola Peninsula, Russia: emphasis on alteration features. *Lithos* **43**, 109–134.
- AKBULUT, M., PIŞKIN, Ö. & KARAYİĞİT, A. (2006): The genesis of the carbonatized and silicified ultramafics known as listvenites: a case study from the Mihaliççik region (Eskişehir), NW Turkey. *Geol. J.* **41**, 557–580.
- ALT, J.C. (1999): Hydrothermal alteration and mineralization of oceanic crust: mineralogy, geochemistry, and processes. In *Volcanic Associated Massive Sulphide Deposits* (T. Barrie & M. Hannington, eds.). *Rev. Econ. Geol.* **8**, 133–155.
- ALT, J.C. & HONNOREZ, J. (1984): Alteration of the upper oceanic crust, DSDP site 417: mineralogy and chemistry. *Contrib. Mineral. Petrol.* **87**, 149–169.
- ALT, J.C., LAVERNE, C., VANKO, D.A., TARTAROTTI, P., TEAGLE, D.A.H., BACH, W., ZULEGER, E., ERZINGER, J., HONNOREZ, J., PEZARD, P.A., BECKER, K., SALISBURY, M.H. & WILKENS, R.H. (1996): Hydrothermal alteration of a section of upper oceanic crust in the eastern equatorial Pacific: a synthesis of results from Site 504B (DSDP legs 69, 70, and 83, and ODP legs 111, 137, 140, and 148). *Proc. ODP, Sci. Results* **148**, 417–434.
- ALT, J.C., TEAGLE, D.A.H., BREWER, T., SHANKS, W.C., III & HALLIDAY, A.N. (1998): Alteration and mineralization of an oceanic fore-arc and the ophiolite – ocean crust analogy. *J. Geophys. Res.* **103**, 12365–12380.
- ASH, C.H. (2001): Relationship between ophiolites and gold–quartz veins in the North American Cordillera. *Department of Energy, Mines and Petroleum Resources, Mineral. Div. Geol. Surv. Branch, Bull.* **108**.
- ASH, C.H. & ARKSEY, R.L. (1990a): The listwanite – lode gold association in British Columbia. In *Geological Fieldwork 1989, A summary of Field Activities and Current Research, Province of British Columbia. Mineral. Res. Div., Geol. Surv. Branch*, 359–364.
- ASH, C.H. & ARKSEY, R.L. (1990b): The Atlin ultramafic allochthon: ophiolitic basement within the Cache Creek terrane, tectonic and metallogenic significance (104N/12). *Geological Fieldwork 1989, A summary of Field Activities and Current Research, Province of British Columbia, Mineral. Res. Div., Geol. Surv. Branch*, 365–374.
- AUCLAIR, M., GAUTHIER, M., TROTTIER, J., JÉBRAK, M. & CHARTRAND, F. (1993): Mineralogy, geochemistry, and paragenesis of the Eastern Metals serpentinite-associated Ni–Cu–Zn deposit, Quebec Appalachians. *Econ. Geol.* **88**, 123–138.
- AYDAL, D. (1990): Gold-bearing listwaenites in the Araç Masif, Kastamonu, Turkey. *Terra Nova* **2**, 43–52.
- BACH, W., ALT, J.C., NIU, YAOLING, HUMPHRIS, S.E., ERZINGER, J. & DICK, H.J.B. (2001): The geochemical consequences of late-stage low-grade alteration of lower ocean crust at the SW Indian Ridge: results from ODP Hole 735B (Leg 176). *Geochim. Cosmochim. Acta* **65**, 3267–3287.
- BAILEY, S.W. (1988): Chlorites: structures and crystal chemistry. In *Hydrous Phyllosilicates* (Exclusive of Micas) (S.W. Bailey, ed.). *Rev. Mineral.* **19**, 347–403.
- BALL, J.W. & NORDSTROM, D.K. (1998): Critical-evaluation and selection of standard state thermodynamic properties for chromium metal and its aqueous ions; hydrolysis species; oxides; and hydroxides. *J. Chem. Eng. Data* **43**, 895–918.

- BERGER, J., FÉMÉNIAS, O., MERCIER, J.C.C. & DEMAÏFFE, D. (2005): Ocean-floor hydrothermal metamorphism in the Limousin ophiolites (western French Massif Central): evidence of a rare preserved Variscan oceanic marker. *J. Metam. Geol.* **23**, 795-812.
- BERMAN, R.G. (1991): Thermobarometry using multi-equilibrium calculations; a new technique, with petrological applications. *Can. Mineral.* **29**, 833-855.
- BERZA, T., BALINTONI, I., IANCU, V., SEGHEDI, A. & HANN, H.P. (1994): South Carpathians. In Geological Evolution of the Alpine – Carpathian – Pannonian system (T. Berza, ed.). ALCAPA II, Field Guidebook. *Rom. J. Tect. Reg. Geol.* **75**, 37-49.
- BERZA, T., KRÄUTNER, H.G. & DIMITRESCU, R. (1983): Nappe structure of the Danubian window of the central South Carpathians. *An. Inst. Geol. Geofiz.* **60**, 31-34.
- BÉZIAT, D., BOURGES, F., DEBAT, P., LOMPO, M., TOLLON, F. & ZONOU, S. (1998): Albitite et "listvenite": sites de concentration aurifère inédits dans les ceintures de roches vertes birimiennes fortement hydrothermalisées du Burkina Faso. *Bull. Soc. Géol. France* **169**, 563-571.
- BISH, D.L. (1977): A spectroscopic and X-ray study of the coordination of Cr<sup>3+</sup> ions in chlorites. *Am. Mineral.* **62**, 385-389.
- BOSCHI, C., FRÜH-GREEN, G.L., DELACOUR, A., KARSON, J.A. & KELLEY, D.S. (2006a): Mass transfer and fluid flow during detachment faulting and development of an oceanic core complex, Atlantis Massif (MAR 30°N). *Geochem. Geophys. Geosyst.* **7**(1), Q01004, doi:10.1029/2005GC001074.
- BOSCHI, C., FRÜH-GREEN, G.L. & ESCARTÍN, J. (2006b): Occurrence and significance of serpentinite-hosted, talc- and amphibole-rich fault rocks in modern oceanic settings and ophiolite complexes: an overview. *Ophioliti* **31**(2), 129-140.
- BUISSON, G. & LEBLANC, M. (1985): Gold in carbonatized ultramafic rocks from ophiolite complexes. *Econ. Geol.* **80**, 2028-2029.
- BUISSON, G. & LEBLANC, M. (1987): Gold in mantle peridotites from Upper Proterozoic ophiolites in Arabia, Mali and Morocco. *Econ. Geol.* **82**, 2091-2097.
- BURKE, T., FAGLIANO, J., GOLDOFT, M., HAZEN, R.E., IGLEWICK, R. & MCKEE, T. (1991): Chromite ore processing residue in Hudson County, New Jersey. *Environm. Health Persp.* **92**, 131-137.
- CANALES, J.P., TUCHOLKE, B.E. & COLLINS, J.A. (2004): Seismic reflection imaging of an oceanic detachment fault: Atlantis megamullion (Mid-Atlantic Ridge, 30°10'N). *Earth Planet. Sci. Lett.* **222**, 543-560.
- CANNAT, M., CEULENEER, G. & FLETCHER, J. (1997): Localization of ductile strain and the magmatic evolution of gabbroic rocks drilled at the Mid-Atlantic Ridge (23°N). *Proc. ODP, Sci. Results* **153**, 77-98.
- CANNAT, M., MÉVEL, C. & STAKES, D. (1991): Normal ductile shear zones at an oceanic spreading ridge: tectonic evolution of Site 735 gabbros (southwest Indian Ocean). *Proc. ODP, Sci. Results* **118**, 415-429.
- CATHELINÉAU, M. (1988): Cation site occupancy in chlorites and illites as a function of temperature. *Clay Mineral.* **23**, 471-485.
- CATHELINÉAU, M. & NIEVA, D. (1985): A chlorite solid solution geothermometer. The Los Azufres (Mexico) geothermal system. *Contrib. Mineral. Petrol.* **91**, 235-244.
- CRAIG, H., BROECKER, W.S. & SPENCER, D. (1981): *GEOSECS Pacific Expedition. 4. Sections and Profiles*. National Science Foundation, Washington, D.C.
- DE CARITAT, P., HUTCHEON, I. & WALSH, J.L. (1993): Chlorite geothermometry: a review. *Clays Clay Minerals* **41**, 219-239.
- DICK, H.J.B., SCHOUTEN, H., MEYER, P.S., GALLO, D.G., BERGH, H., TYCE, R., PATRIAT, P., JOHNSON, K.T.M., SNOW, J. & FISHER, A. (1991): Tectonic evolution of the Atlantis II fracture zone. *Proc. ODP, Sci. Results* **118**, 359-398.
- DILEK, Y., KEMPTON, P.D., THY, P., HURST, S.D., WHITNEY, D. & KELLEY, D.S. (1997): Structure and petrology of hydrothermal veins in gabbroic rocks from sites 921 to 924, Mark area (Leg 153): alteration history of slow-spread lower oceanic crust. *Proc. ODP, Sci. Results* **153**, 155-178.
- DYAR, M.D., GUIDOTTI, C.V., HARPER, G.D., MC KIBBEN, M.A. & SACCOCCIA, P.J. (1992): Controls on ferric iron in chlorite. *Geol. Soc. Am., Abstr. Programs* **24**, 130.
- ESCARTIN, J., MÉVEL, C., MACLEOD, C.J. & MCCAIG, A.M. (2003): Constraints on deformation conditions and the origin of oceanic detachments: the Mid-Atlantic Ridge core complex at 15°45'N. *Geochem. Geophys. Geosystems* **4**(8), 1067, doi:10.1029/2002GC000472.
- FÉMÉNIAS, O. (2003): *Contribution à l'étude du magmatisme tardi- à post-orogénique, de sa source à sa mise en place en sub-surface: exemples régionaux de l'essai de filons du Motru (Roumanie) et du complexe lité profond sous Beaunit (France)*. Ph.D. thesis, Université Libre de Bruxelles, Belgique.
- FÉMÉNIAS, O., BERZA, T., TATU, M., DIOT, H. & DEMAÏFFE, D. (2008): Nature and significance of a Cambro-Ordovician high-K calc-alkaline sub-volcanic suite: the late- to post-orogenic Motru dyke swarm (southern Carpathians, Romania). *Int. J. Earth Sci.* **97**, 479-496.
- FENDORF, S.E. (1995): Surface reactions of chromium in soils and waters. *Geoderma* **67**(1-2), 55-71.
- FLETCHER, J.M., STEPHENS, C.J., PETERSEN, E.U. & SKERL, L. (1997): Greenschist facies hydrothermal alteration of oce-

- anic gabbros: a case study of element mobility and reaction paths. *Proc. ODP, Sci. Results* **153**, 389-398.
- FOSTER, M.D. (1962): Interpretation of the composition and a classification of the chlorites. *U.S. Geol. Surv., Prof. Pap.* **414-A**.
- FRANZ, G. & LIEBSCHER, A. (2004): Physical and chemical properties of the epidote minerals – an introduction. In *Epidotes* (A. Liebscher & G. Franz, eds.). *Rev. Mineral. Geochem.* **56**, 1-81.
- GARDIEN, V., LE GALL, B., CÉLÉRIER, B., LOUVEL, V. & HUCHON, P. (2002): Low pressure-temperature evolution of the continental crust exhumed during the opening of the Woodlark Basin. *Proc. ODP, Sci. Results* **180**, 1-28.
- GIRARDEAU, J. & MÉVEL, C. (1982): Amphibolitized sheared gabbros from the ophiolites as indicators of the evolution of the oceanic crust: Bay of Islands, Newfoundland. *Earth Planet. Sci. Lett.* **61**, 151-165.
- GRAHAM, I.T., FRANKLIN, B.J. & MARSHALL, B. (1996): Chemistry and mineralogy of podiform chromitite deposits, southern NSW, Australia: a guide to their origin and evolution. *Mineral. Petrol.* **57**, 129-150.
- GUIDOTTI, C.V. & SASSI, F.P. (1998): Miscellaneous isomorphous substitutions in Na–K white micas: a review, with special emphasis to metamorphic micas. *Rend. Fis. Accad. Lincei, ser. 9*, **9**, 57-78.
- GUIDOTTI, C.V., YATES, M.G., DYAR, M.D. & TAYLOR, M.E. (1994): Petrogenetic significance of the Fe<sup>3+</sup> content of muscovite in pelitic schists. *Am. Mineral.* **79**, 793-795.
- GURAU, A., VISOIU, I. & SCARLAT, L. (1976): Prezentă fuchsitului în gabbrourele de Plavisevita, Muntiu Almajului, Banatul de Sud. In *Dari de Seama ale Sedintelor - Institutul de Geologie și Geofizică*, **63**, 1. Mineralogie-Petrologie-Geochemie, 37-50.
- HALLS, C. & ZHAO, R. (1995): Listvenite and related rocks: perspectives on terminology and mineralogy with reference to an occurrence at Cregganbaun, Co. Mayo, Republic of Ireland. *Mineral. Deposita* **30**, 303-313.
- HAMLIN, P.R. (1975): Chromite alteration in the Pantou sill, East Kimberley region, Western Australia. *Mineral. Mag.* **40**, 181-192.
- HARLOW, G.E. (1995): Crystal chemistry of barium enrichment in micas from metasomatized inclusions in serpentinites, Motagua Fault Zone, Guatemala. *Eur. J. Mineral.* **7**, 775-789.
- HILLIER, S. & VELDE, B. (1991): Octahedral occupancy and the chemical composition of diagenetic (low-temperature) chlorites. *Clay Minerals* **26**, 149-168.
- HONNOREZ, J. (2003): Hydrothermal alteration vs. ocean-floor metamorphism. A comparison between two case histories: the TAG hydrothermal mound (Mid-Atlantic Ridge) vs. DSDP/ODP Hole 504B (Equatorial East Pacific). *C.R. Geoscience* **335**, 781-824.
- HOPKINSON, L., BEARD, J.S. & BOULTER, C.A. (2004): The hydrothermal plumbing of a serpentinite-hosted detachment: evidence from the West Iberia non-volcanic rifted continental margin. *Marine Geol.* **204**, 301-315.
- HOPKINSON, L. & ROBERTS, S. (1995): Ridge axis deformation and coeval melt migration within layer 3 gabbros: evidence from the Lizard Complex, U.K. *Contrib. Mineral. Petrol.* **121**, 126-138.
- JIANG, WEI-TEH, PEACOR, D.R. & BUSECK, P.R. (1994): Chlorite geothermometry? Contamination and apparent octahedral vacancies. *Clays Clay Minerals* **42**, 593-605.
- JOWETT, E.C. (1991): Fitting iron and magnesium into the hydrothermal chlorite geothermometer. *Geol. Assoc. Can. – Mineral. Assoc. Can. – Soc. Econ. Geol., Program Abstr.* **16**, A62.
- KARSON, J.A. & LAWRENCE, R.M. (1997): Tectonic window into gabbroic rocks of the middle oceanic crust in the MARK area near Sites 921-924. *Proc. ODP, Sci. Results* **153**, 61-76.
- KIMBALL, K.L. (1990): Effects of hydrothermal alteration on the compositions of chromian spinels. *Contrib. Mineral. Petrol.* **105**, 337-346.
- KISHIDA, A. & KERRICH, R. (1987): Hydrothermal alteration zoning and gold concentration at the Kerr–Addison Archean lode gold deposit, Kirkland Lake, Ontario. *Econ. Geol.* **82**, 649-690.
- KITAJIMA, K., MARUYAMA, S., UTSUNOMIYA, S. & LIOU, J.G. (2001): Seafloor hydrothermal alteration at an Archean mid-ocean ridge. *J. Metam. Geol.* **19**, 583-599.
- KLEMD, R. (2004): Fluid inclusions in epidote minerals and fluid development in epidote-bearing rocks. In *Epidotes* (A. Liebscher & G. Franz, eds.). *Rev. Mineral. Geochem.* **56**, 197-234.
- KOÇ, S. & KADIOĞLU, Y. (1996): Mineralogy, geochemistry and precious metal content of Karacakaya (Yunusremre–Eskisehir) listwaenites. *Oftoliti* **21**(2), 125-130.
- KRANIDIOTIS, P. & MACLEAN, W.H. (1987): Systematics of chlorite alteration at the Phelps Dodge massive sulfide deposit, Matagami, Quebec. *Econ. Geol.* **82**, 1898-1911.
- KRÄUTNER, H., NASTASEANU, S., BERZA, T., STANOIU, I. & IANCU, V. (1981): Metamorphosed Paleozoic in the South Carpathians and its relation to the pre-Paleozoic basement. *Carpath. Balkan. Assoc. Congress XII (Bucaresti), Guide to Excursion A*.
- LEAKE, B.E., WOOLLEY, A.R., ARPS, C.E.S., BIRCH, W.D., GILBERT, M. C., GRICE, J.D., HAWTHORNE, F.C., KATO, A., KISCH, H.J., KRIVOVICHEV, V.G., LINTHOUT, K., LAIRD, J., MANDARINO, J.A., MARESCH, W.V., NICKEL, E.H., ROCK, N.M.S., SCHUMACHER, J. C., SMITH, D.C., STEPHENSON,

- N.C.N., UNGARETTI, L., WHITTAKER, E.J.W. & GUO YOUZHI (1997): Nomenclature of amphiboles: report of the Subcommittee on Amphiboles of the International Mineralogical Association Commission on New Minerals and Mineral Names. *Mineral. Mag.* **61**, 295-321.
- LÉCUYER, C., BROUXEL, M. & ALBARÈDE, F. (1990): Elemental fluxes during hydrothermal alteration of the Trinity ophiolite (California, U.S.A.) by seawater. *Chem. Geol.* **89**, 87-115.
- LEMOINE, M., TRICART, P. & BOILLOIT, G. (1987): Ultramafic and gabbroic ocean floor of the Ligurian Tethys (Alps, Corsica, Apennines): in search for a genetic model. *Geology* **15**, 622-625.
- LIU, J.G. & ERNST, W.G. (1979): Oceanic ridge metamorphism of the East Taiwan ophiolite. *Contrib. Mineral. Petrol.* **68**, 335-348.
- LIU, J.G., KUNIYOSHI, S. & ITO, K. (1974): Experimental studies of the phase relations between greenschist and amphibolite in a basaltic system. *Am. J. Sci.* **274**, 613-632.
- MANATSCHAL, G. & MÜNTENER, O. (2008): A type sequence across an ancient magma-poor ocean-continent transition: the example of the western Alpine Tethys ophiolites. *Tectonophysics*, doi:10.1016/j.tecto.2008.07.021.
- MĂRUNTU, M. (1984): Inner structure and petrology of Tisovita-Iuți ophiolitic complex (Almaj Mountains). *St. Cerc. Geol. Geofiz. Geogr., Geologie*, **29**, 44-54 (in Romanian, with English abstr.).
- MĂRUNTU, M., MENOT, R.P. & TAPARDEL, C. (1997): Cryptic variation and geochemistry of cumulate pile from Tisovita-Iuți ophiolite: preliminary approach of magma chamber evolution and tectonic setting. *In* Int. Symp. Geology in the Danubian Gorges Orsova, Yugoslavia and Romania, Donji Milanovac \* 23-26 IX, 295-299.
- MELLINI, M., RUMORI, C. & VITI, C. (2005): Hydrothermally reset magmatic spinels in retrograde serpentinites: formation of "ferritchromit" rims and chlorite aureoles. *Contrib. Mineral. Petrol.* **149**, 266-275.
- MÉVEL, C. (1988): Metamorphism in oceanic layer 3, Goringe Bank, Eastern Atlantic. *Contrib. Mineral. Petrol.* **100**, 496-509.
- MÉVEL, C., CABY, R. & KIENAST, J.-R. (1978): Amphibolite-facies conditions in the oceanic crust: example of amphibolitized fiaser-gabbro and amphibolites from the Chenaillat ophiolite massif (Hautes Alpes, France). *Earth Planet. Sci. Lett.* **39**, 98-108.
- MÉVEL, C. & KIENAST, J.R. (1980): Chromian jadeite, phengite, pumpellyite, and lawsonite in a high-pressure metamorphosed gabbro from the French Alps. *Mineral. Mag.* **43**, 979-984.
- MITRA, S., PAL, T., MAITY, P.K. & MOON, H.-S. (1992): Ferritchromit and its opto-chemical behaviour. *Mineral. J.* **16**, 173-186.
- MUSSALLAM, K., JUNG, D. & BURGATH, K. (1981): Textural features and chemical characteristics of chromites in ultramafic rocks, Chalkidiki Complex (northeastern Greece). *Tschermaks Mineral. Petrogr. Mitt.* **29**, 75-101.
- NASIR, S., AL SAYIGH, A.R., AL HARTHY, A., AL-KHIRBASH, S., AL-JAAIDI, O., MUSLLAM, A., AL-MISHWAT, A. & AL-BU'SAIDI, S. (2007): Mineralogical and geochemical characterization of listwaenite from the Semail ophiolite, Oman. *Chem. Erde Geochem.* **67**, 213-228.
- NIMIS, P., TESALINA, S.G., OMENETTO, P., TARTAROTTI, P. & LEROUGE, C. (2004): Phyllosilicate minerals in the hydrothermal mafic-ultramafic-hosted massive-sulfide deposit of Ivanovka (southern Urals): comparison with modern ocean seafloor analogues. *Contrib. Mineral. Petrol.* **147**, 363-383.
- NIXON, G.T. (1990): Geology and precious metal potential of mafic-ultramafic rocks in British Columbia: current progress. *In* Geological Fieldwork 1989. B.C. Ministry of Energy, Mines and Petroleum Resources, *Pap.* **1990-1**, 353-358.
- OZE, C.J.-P. (2003): *Chromium Geochemistry of Serpentinites and Serpentine Soils*. Ph.D. thesis, Stanford Univ., Stanford, California.
- PARRA, T., VIDAL, O. & AGARD, P. (2002): A thermodynamic model for Fe-Mg dioctahedral K white micas using data from phase-equilibrium experiments and natural pelitic assemblages. *Contrib. Mineral. Petrol.* **143**, 706-732.
- PHILLIPS, T.L., LOVELESS, J.K. & BAILEY, S.W. (1980): Cr<sup>3+</sup> coordination in chlorites: a structural study of ten chromian chlorites. *Am. Mineral.* **65**, 112-122.
- PLISSART, G., DIOT, H., MARUNTU, M., FÉMÉNIAS, O., BERZA, T. & LAUNNEAU, P. (2007): Syn-orogenic granitic magma emplacement during transpressional phase: the Variscan Cherbelez Massif (southern Carpathians, Romania). *3MA Int. Symp. (Fez, Morocco)*, *Abstr.*
- RIEDER, M., CAVAZZINI, G., D'YAKONOV, Y.S., FRANK-KAMENETSKII, V.A., GOTTARDI, G., GUGGENHEIM, S., KOVAL, P.V., MÜLLER, G., NEIVA, A.M.R., RADOSLOVICH, E.W., ROBERT, J.-L., SASSI, F.P., TAKEDA, H., WEISS, Z. & WONES, D.R. (1998): Nomenclature of the micas. *Can. Mineral.* **36**, 41-48.
- ROBINSON, P.T., ERZINGER, J. & EMMERMANN, R. (2002): The composition and origin of igneous and hydrothermal veins in the lower ocean crust - ODP Hole 735B, Southwest Indian Ridge. *Proc. ODP, Sci. Results* **176**, 1-66.
- ROSE, G. (1837): *Mineralogisch-geognostische Reise nach dem Ural, dem Altai und dem Kaspischen Meere. I. Reise nach dem nördlichen Ural und dem Altai*. C.W. Eichhoff (Verlag der Sanderschen Buchhandlung), Berlin, Germany.
- RULE, A.C. & BAILEY, S.W. (1987): Refinement of the crystal structure of a monoclinic ferroan clinocllore. *Clays Clay Minerals* **35**, 129-138.

- SCHROEDER, T. & JOHN, B.E. (2004): Strain localization on an oceanic detachment fault system, Atlantis Massif, 30°N, Mid-Atlantic Ridge. *Geochem. Geophys. Geosystems* **5**(11), Q11007, doi:10.1029/2004GC000728.
- SEARLE, R.C. & ESCARTIN, J. (2004): The rheology and morphology of oceanic lithosphere and mid-ocean ridges. In *Mid-Ocean Ridges: Hydrothermal Interactions Between the Lithosphere and Oceans* (C.R. German, J. Lin & L.M. Parson, eds.). *Am. Geophys. Union, Geophys. Monogr. Ser.* **148**, 63–93.
- SHAU, YEN-HONG, PEACOR, D.R. & ESSENE, E.J. (1990): Corrensite and mixed-layer chlorite/corrensite in metabasalt from northern Taiwan: TEM/AEM, EMPA, XRD, and optical studies. *Contrib. Mineral. Petrol.* **105**, 123–142.
- SHEN, POUYAN, HWANG, SHYH-LUNG, CHU, HAO-TSU & JENG, RUEY-CHANG (1988): STEM study of “ferritchromit” from the Heng–Chun chromitite. *Am. Mineral.* **73**, 383–388.
- STAKES, D., MÉVEL, C., CANNAT, M. & CHAPUT, T. (1991): Metamorphic stratigraphy of Hole 735B. *Proc. ODP, Sci. Results* **118**, 153–180.
- STĂNOIU, I. (1973): Zona Mehedinți–Retezat: o unitate paleogeografică și tectonică a Carpatilor Meridionali. *D.S. Inst. Geol.* **LIX**(5), 127.
- STORRE, B. & NITSCH, K.-H. (1972): Die Reaktion  $2 \text{Zoisit} + 1 \text{CO}_2 = 3 \text{Anorthit} + 1 \text{Calcit} + 1 \text{H}_2\text{O}$ . *Contrib. Mineral. Petrol.* **35**, 1–10.
- TALBI, E.L.H., HONNOREZ, J., CLAUER, N., GAUTHIER-LAFAYE, F. & STILLE, P. (1999): Petrology, isotope geochemistry and chemical budgets of oceanic gabbros – seawater interactions in the Equatorial Atlantic. *Contrib. Mineral. Petrol.* **137**, 246–266.
- TRELOAR, P.J. (1987): The Cr-minerals of Outokumpu – their chemistry and significance. *J. Petrol.* **28**, 867–886.
- TREVES, B.E. & HARPER, G.H. (1994): Exposure of serpentinites on the ocean floor: sequence of faulting and hydrofracturing in the Northern Apennine ophiolites. *Ophioliti* **19b**, 435–466.
- TSIKOURAS, B., KARIPL, S., GRAMMATIKOPOULOS, T. & HATZIPANAGIOTOU, K. (2006): Listwaenite evolution in the ophiolite mélange of Iti Mountain (continental central Greece). *Eur. J. Mineral.* **18**, 243–255.
- UÇURUM, A. (1998): Application of the correspondence-type geostatistical analysis on the Co, Ni, As, Ag and Au concentrations of the listwaenites from serpentinites in the Divriği and Kuluncak ophiolitic mélanges. *Turkish J. Earth Sci.* **7**(2), 87–95.
- UÇURUM, A. (2000): Listwaenites in Turkey: perspectives on formation and precious metal concentration with reference to occurrences in east-central Anatolia. *Ophioliti* **25**(1), 15–29.
- VAN DER WEIJDEN, C.H. & REITH, M. (1982): Chromium(III) – chromium(VI) interconversions in seawater. *Marine Chem.* **11**, 565–572.
- VANKO, D.A. & STAKES, D.S. (1991): Fluids in oceanic layer 3: evidence from veined rocks, Hole 735B, Southwest Indian Ridge. *Proc. ODP, Sci. Results* **118**, 181–215.
- VELDE, B. (1967): Si<sup>4+</sup> content of natural phengites. *Contrib. Mineral. Petrol.* **14**, 250–258.
- VIDAL, O., DE ANDRADE, V., LEWIN, E., MUNOZ, M., PARRA, T. & PASCARELLI, S. (2006): P–T–deformation–Fe<sup>3+</sup>/Fe<sup>2+</sup> mapping at the thin section scale and comparison with XANES mapping. Application to a garnet-bearing metapelite from the Sambagawa metamorphic belt (Japan). *J. Metam. Geol.* **24**, 669–683.
- VIDAL, O. & PARRA, T. (2000): Exhumation paths of high pressure metapelites obtained from local equilibria for chlorite–phengite assemblages. *Geol. J.* **35**, 139–161.
- VIDAL, O., PARRA, T. & TROTET, F. (2001): A thermodynamic model for Fe–Mg aluminous chlorite using data from phase equilibrium experiments and natural pelitic assemblages in the 100–600°C, 1 to 25 kbar range. *Am. J. Sci.* **301**, 557–592.
- VIDAL, O., PARRA, T. & VIEILLARD, P. (2005): Thermodynamic properties of the Tschermak solid solution in Fe–chlorite: application to natural examples and possible role of oxidation. *Am. Mineral.* **90**, 347–358.
- WHITMORE, D.R.E., BERRY, L.G. & HAWLEY, J.E. (1946): Chrome micas. *Am. Mineral.* **31**, 1–21.
- WINCHESTER, J.A. & MAX, M.D. (1984): Element mobility associated with syn-metamorphic shear zones near Scotchport, N.W. Mayo, Ireland. *J. Metam. Geol.* **2**, 1–11.
- ZAKARIADZE, G.S., BAYANOVA, T.B. & KARPENKO, S.F. (2006): Age, composition and origin of the paleoceanic gabbros of Deli Jovan massif (NE Serbia). *Ophioliti* **31**(2), 223–224.
- ZANE, A., SASSI, R. & GUIDOTTI, C.V. (1998): New data on metamorphic chlorite as a petrogenetic indicator mineral, with special regard to greenschist-facies rocks. *Can. Mineral.* **36**, 713–726.
- ZANG, W. & FYFE, W.S. (1995): Chloritization of the hydrothermally altered bedrock at the Igarapé Bahia gold deposit, Carajás, Brazil. *Mineral. Deposita* **30**, 30–38.
- ZHARIKOV, V.A., PERTSEV, N.N., RUSINOV, V.L., CALLEGARI, E. & FETTES, D.J. (2007): A systematic nomenclature for metamorphic rocks. 9. Metasomatism and metasomatic rocks. In *Recommendations by the IUGS Subcommission on the Systematics of Metamorphic Rocks* (SCMR website: www.bgs.ac.uk/scmr).

Received May 6, 2008, revised manuscript accepted February 3, 2009.

